

Design and Implementation of Controller for BLDC Machine using PIC Microcontroller

A Project Report

submitted by

DHINESH KUMAR S

*in partial fulfilment of the requirements
for the award of the degree of*

MASTER OF TECHNOLOGY



**DEPARTMENT OF ELECTRICAL ENGINEERING
INDIAN INSTITUTE OF TECHNOLOGY MADRAS.**

MAY 2014

THESIS CERTIFICATE

This is to certify that the thesis titled **Design and Implementation of Controller for BLDC machine using PIC Microcontroller**, submitted by **DHINESH KUMAR S**, to the Indian Institute of Technology, Madras, for the award of the degree of **MASTER OF TECHNOLOGY**, is a bona fide record of the research work done by him under our supervision. The contents of this thesis, in full or in parts, have not been submitted to any other Institute or University for the award of any degree or diploma.

Dr.N.Lakshmi Narasamma
Assistant Professor
Dept. of Electrical Engineering
IIT Madras - 600 036

Place: Chennai

May 17, 2014

ACKNOWLEDGEMENTS

I take this opportunity to thank TVS Motor Company for sponsoring me in pursuing Master of Technology at Indian Institute of Technology, Madras. It gives me a lot of new learning experiences and exposure to new world of technology.

I am deeply grateful to Dr.Lakshmi Narasamma, Assistant Professor, IIT Madras, who guides me throughout my project work and took the best out of me. The project work not only concentrated on single domain but also gives experience in several fields.

I express my gratitude to Dr.Krishna Vasudevan, Dr.Srirama Srinivas, Dr.Kamalesh Hatua and Technical staffs in our department. They guided me with technical reasons and put me in the right direction, whenever I am struggling to get things done. The support and real motivation, provided by them makes me confident and improve my level of understanding.

I am thankful to Research scholars in my lab, particularly, Mr.Krishna Teja Orrey, Mr.Sandeep Kolluri, Mr.Kedarnath, Mr.Lokesh and my fellow classmates. They give me immense support in all paradigms, throughout my stay in IIT Madras.

ABSTRACT

KEYWORDS: BLDC ; Speed control; Simulation; Hardware.

Brushless DC machines has high power to volume ratio and characteristics similar to conventional DC machines. They require power electronic control for operating the machine. The control of machines is more accurate and high speed of response can be achieved although control structure and algorithms are complex. The implementation of digital controller make complex manipulations of machine equations within very short time and had better noise rejection filters. The major drawback of implementing digital controller is the limited bandwidth. BLDC machines, characterized by trapezoidal back-emf, which are also called as commutator-less DC machines, has two modes of operation. Sensored and sensorless operation, each has its own merits and demerits. In Sensorless mode, there are various ways to sense the position of rotor and among those, sensing phase back-emf is the widely used and older method.

This project emphasises on development of low-cost controller and power circuit used for driving BLDC motors which can be implemented in laboratory for demonstration. Also, the speed control of BLDC motor in sensorless mode using microcontroller.

TABLE OF CONTENTS

ACKNOWLEDGEMENTS	i
ABSTRACT	ii
LIST OF TABLES	vi
LIST OF FIGURES	ix
ABBREVIATIONS	x
NOTATION	xi
1 Introduction	1
1.1 Classification of Motors	1
1.2 Permanent Magnet Machines	3
1.2.1 Classification of Permanent Magnet Machines	3
1.2.1.1 Permanent Magnet DC machines	3
1.2.1.2 Permanent Magnet AC machines	3
1.3 Advantages of BLDC machine over Conventional DC machine . . .	4
1.4 Construction and Operation of BLDC machine	4
1.4.1 Stator	4
1.4.2 Rotor	5
1.4.3 Hall sensors	6
1.4.4 Operation of BLDC motor	7
1.5 Theoretical Understanding of BLDC machine model	12
1.6 Organization of Project Report	14
2 Design of Controller and Simulation Results	15
2.1 Simulation Results of BLDC machine in Open loop	15

2.1.1	Sensored Operation in Open loop	15
2.1.2	Sensorless Operation in Open loop	17
2.2	Design of Controller	19
2.2.1	DC Link Voltage Control	19
2.2.2	Pulse Width Modulation Control	19
2.2.3	Hysteresis Control	20
2.2.4	Machine parameters	20
2.2.5	Design of Current Controller	21
2.2.6	Design of Speed Controller	25
2.3	Simulation Results of BLDC machine in Closed loop	28
3	Hardware Implementation	32
3.1	Introduction	32
3.2	Design of Controller Circuit	33
3.2.1	Selection of Microcontroller and its Powering modes	34
3.2.1.1	Powering Modes of Microcontroller	34
3.2.1.2	Description about MPLAB X IDE software	35
3.3	Design of LCD interface	36
3.4	Implementation of Frequency to Voltage converter	36
3.5	Software Implementation	37
3.6	Design of Inverter Circuit	38
3.6.1	Design Consideration for transistor driver configuration in BLDC Inverter Circuit	43
3.6.2	Design of Current sense resistor	46
3.6.3	Design of DC bus Capacitance	48
3.6.4	Design of Back-EMF sensing circuit	48
3.6.5	Design of Inverter Printed Circuit Board	49
3.6.6	Selection of BLDC motor	50
3.7	Model Validation and Experimental Results	51
3.7.1	Observations and Learning outcomes from Experiments	52
3.7.1.1	Condition: Sensorless open loop	52

3.7.1.2	Condition : Sensorless Mode of operation in closed loop with No load	54
3.7.1.3	Condition : Sensorless mode of operation in closed loop with load	54
4	Summary and Future Scope	57
4.1	Summary	57
4.2	Future Scope	57
A	Motor Specifications	59
B	Circuit Block Diagram	60
C	Inverter Schematic	61
D	Controller Schematic	62
E	Bill of Materials for Driver Circuit	63
F	Bill of Materials for Controller Circuit	64
G	N Channel MOSFET	65
H	P Channel MOSFET	66

LIST OF TABLES

1.1	Commutation Sequence based on Hall Sensor outputs	7
2.1	Comparison of sensored and sensorless operation	17
3.1	Comparison of features of Microcontroller among different manufacturers	34
3.2	Selection of Current sense resistor value	47
3.3	Placement of Current sense Resistor	47

LIST OF FIGURES

1.1	Classification of Motors	2
1.2	Connection diagram of Stator winding	5
1.3	Surface-Mount Rotor BLDC	5
1.4	Inset Mount Rotor BLDC	6
1.5	Buried PM Rotor BLDC	6
1.6	Operation of BLDC machine	7
1.7	Ideal case waveforms Back-EMF and Phase current for 360°	8
1.8	Equivalent circuit of BLDC machine when B and C phases are conducting and A phase freewheeling	9
1.9	Back-EMF and Phase current for 360°	10
1.10	Waveforms describing BLDC operation	13
1.11	Waveforms of BLDC operation in PWM mode	14
2.1	Sensored Operation of BLDC in open loop	16
2.2	Sensored Operation of BLDC in open loop under loaded condition	17
2.3	Sensorless Operation of BLDC in open loop	18
2.4	Block Diagram of Complete Controller Design	20
2.5	Plant structure including electrical and mechanical	21
2.6	Bode Diagram for Plant transfer function	22
2.7	Implementation of Current Controller	23
2.8	Bode Diagram for Compensated Loop gain function of inner current loop	24
2.9	Step response of inner current loop	25
2.10	Implementation of Speed Controller	25
2.11	Bode Diagram for Mechanical system transfer function	26
2.12	Bode Diagram for Compensated Loop gain function of outer speed loop	28
2.13	Step response of outer speed loop	29

2.14	Sensored Operation of BLDC in Closed loop with $V_{dc} = 12\text{ V}$ and $T_l = 0.1\text{ Nm}$	30
2.15	Sensored Operation of BLDC in Closed loop with $V_{dc} = 12\text{ V}$ and $T_l = 0.26\text{ Nm}$	31
3.1	Hardware Board of Controller circuit	33
3.2	Powering Options of Microcontroller	35
3.3	Basic Gate Pulse from microcontroller Scale x-axis - $10\text{ }\mu\text{s/div}$ y-axis - 1 V/div	36
3.4	Main Procedure for running experiment	38
3.5	Algorithm for Main loop	39
3.6	Algorithm for Interrupt Service Routine loop	40
3.7	Typical 2-level Voltage Source Inverter	41
3.8	Gate Turn-ON characteristics of N-channel MOSFET Scale x-axis - $10\text{ }\mu\text{s/div}$ y1-axis - 1 V/div y2-axis - 1 V/div	42
3.9	Gate Turn-ON characteristics of P-channel MOSFET Scale x-axis - 1 ms/div y-axis - 2 V/div y2-axis - 1 V/div	42
3.10	Transistor Driver circuit for MOSFETs	43
3.11	Driver output with respect to gate pulse Scale x-axis - 20 ms/div y-axis - 2 V/div	44
3.12	Schematic Diagram of Current sensing	48
3.13	Schematic Diagram of Back EMF sensing	49
3.14	Hardware Board of Inverter circuit	50
3.15	Complete Experimental set-up	51
3.16	Motor loading arrangement	52
3.17	Simulation and Hardware results comparison of Motor RPM	52
3.18	Motor Excitation current and Back EMF Voltage	53
3.19	Simulation and Hardware results comparison of square wave input gate pulse	53
3.20	Simulation and Hardware results comparison of PWM duty to gate pulses	54
3.21	Sensorless Operation of BLDC in Closed loop with $V_{dc} = 12\text{ V}$	55
3.22	Simulation and Hardware results comparison	56
3.23	Simulation and Hardware results comparison in loaded condition	56

A.1	Motor Specification	59
B.1	Complete Circuit Block Diagram	60
C.1	Inverter Schematic for BLDC Drive	61
D.1	Controller Schematic for BLDC Drive	62
E.1	BOM for Driver Circuit	63
F.1	BOM for Controller Circuit	64
G.1	Specifications of N-Channel MOSFET	65
H.1	Specifications of P-Channel MOSFET	66

ABBREVIATIONS

BLDC	Brushless Direct Current
PM	Permanent Magnet
ANSI	American National Standards Institute
IEEE	Institute of Electrical and Electronics Engineers
NEMA	National Electrical Manufacturers Association
EMF	Electromotive Force
MATLAB	Matrix Laboratory
RAM	Random Access Memory
ADC	Analog to Digital Converter
LCD	Liquid Crystal Display
SPI	Serial Parallel Interface
I2C	Inter-Inter Communication
EUSART	Enhanced Universal Synchronous Asynchronous Receiver Transmitter
MOSFET	Metal Oxide Field Effect Transistor
IGBT	Insulated Gate Bipolar Transistor
KVL	Kirchoff's Voltage Law
PCB	Printed Circuit Board
ICD	IN-Circuit Debugger
ICSP	In-Circuit Serial Programming
IDE	Integrated Development Environment
PWM	Pulse Width Modulation
LED	Light Emitting Diode
ISR	Interrupt Service Routine
PC	Personal Computer
RPM	Revolutions Per Minute
IC	Integrated Circuit

NOTATION

R	Resistance per phase
L	Inductance per phase
H	Hall sensor signal
S	Switch(MOSFET)
PI	Proportional and Integral
V_{dc}	DC source voltage
I_{dc}	Average DC source current
E_b	Average Backemf per phase
k_t	Torque constant
ω_m	Speed in radians
T_e	Electromagnetic torque
T_l	Load torque
i	Instantaneous current
e	Instantaneous backemf
θ	Rotor Electrical angle in degrees
P	Pole pairs
K_p	Proportional constant
K_I	Integral constant
τ_{elec}	Electrical time-constant
τ_{mech}	Mechanical time-constant
τ_{em}	Mechanical time-constant
f_s	Switching Frequency

CHAPTER 1

Introduction

In the modern society, electricity is the most popular secondary energy source. The application of motors had spread to all fields in our daily life and national economy, as mechanical to electrical energy conversion devices. Since its origin, the development of motors, adaptability to different applications had been intensive. The economic constraints and new standards legislated by government place higher requirements of electrical systems. New generation of equipments must have better performance parameters such as high efficiency, high torque to weight ratio and so on. All these parameters should be achieved at decreased system cost. Real-time applications involve precise control and required output from the rotating machine, which provide great challenges to electrical engineers.

1.1 Classification of Motors

Electric motors, which are the most important electrical energy conversion device had been classified vastly based on several criteria.

1. Based on type of Power Source, DC Motors and AC motors.
2. Based on type of motion, Linear and Rotational.
3. Based on type of field excitation, Permanent Magnet and Electromagnet.
4. Based on type of commutator arrangement, Split ring, slip ring and Commutatorless

The figure 1.1 gives us complete classification of motors^[1].

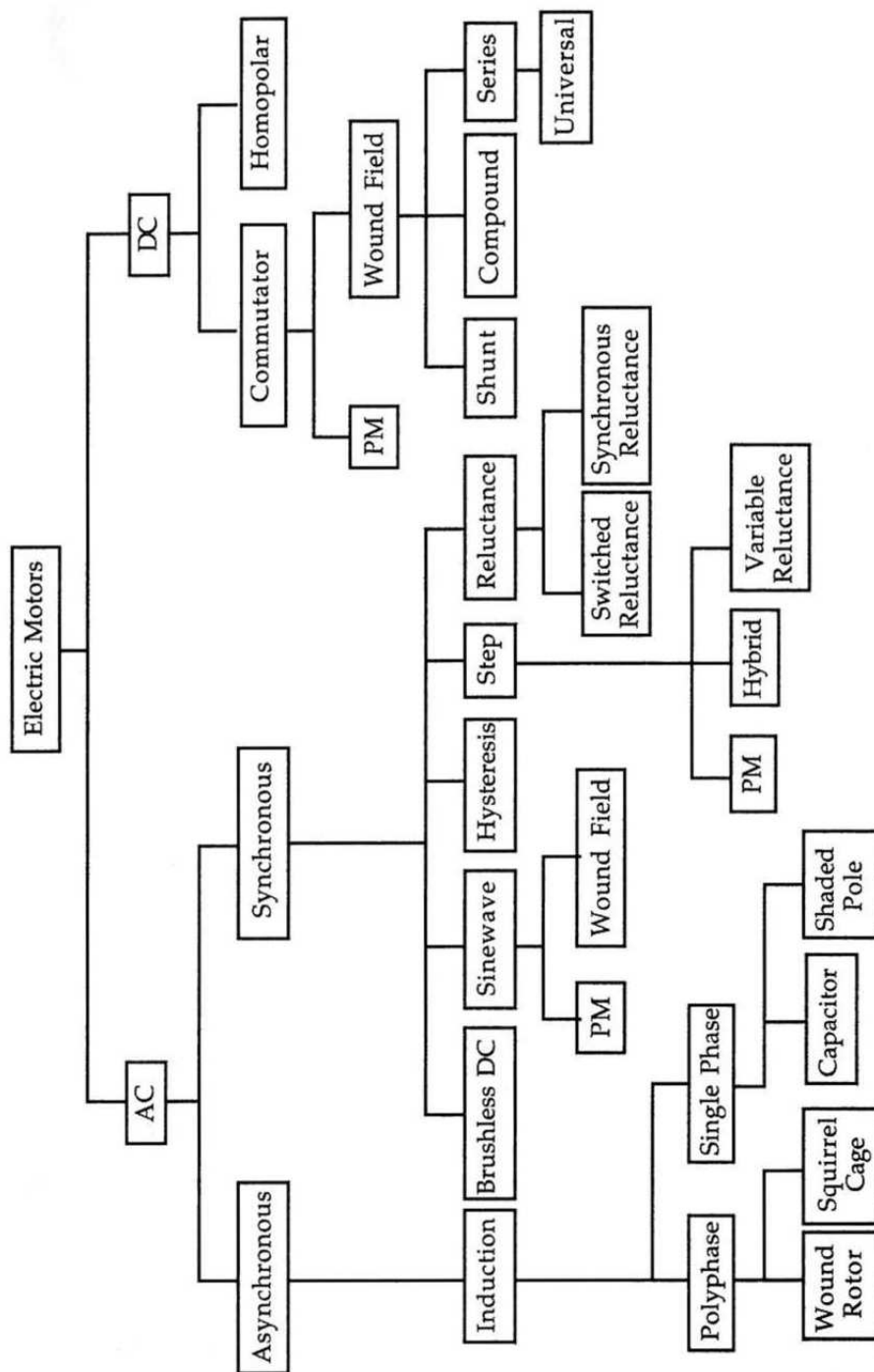


Figure 1.1: Classification of Motors

1.2 Permanent Magnet Machines

Introduction of Permanent magnets resulted in compactness and high power to weight ratio. Though conventional DC machines are highly efficient, the drawback is that they require commutator and brush arrangement which are subjected to arcing and mechanical wear and tear losses. With the rapid development in the field of power electronics, high power and high frequency power semiconductor switches are functionally equivalent to commutator and brush arrangement. But Power switches have their own merits and demerits.

1.2.1 Classification of Permanent Magnet Machines

The main classification of PM machines is based on the placement of Permanent magnets.

1.2.1.1 Permanent Magnet DC machines

In these machines, Permanent magnets are placed in the stator. These machines require commutator and brush arrangement, are provided with DC excitation to the armature. The performance of the machine is comparable to the conventional DC machine.

1.2.1.2 Permanent Magnet AC machines

These machines have permanent magnets placed in the rotor. Also known as Commutator-less Machines. These machines don't require commutator and brush. The position of the rotor is sensed using Hall sensors and AC excitation is provided with the help of inverter. Depending upon the wave shape of back-emf, Permanent Magnet AC machines can be classified into two types.

1. Permanent Magnet Brush-less DC Machines
2. Permanent Magnet Synchronous Machines

As per ANSI/IEEE 100-1984 and NEMA MG7-1987, BLDC machine is a type of self-synchronous rotary motor controlled by electronic commutation, where rotor is mounted with permanent magnets along with rotor position sensors and commutation circuit can either be independent or integrated to the motor.

Depending upon the type of mounting of Permanent magnets in the rotor, PMBLDC machines are classified into two types.

1. Interior mounted
2. Surface mounted

1.3 Advantages of BLDC machine over Conventional DC machine

1. Less Maintenance is required since no commutator and brush.
2. Low rotor inertia since permanent magnets are used.
3. No limitation over speed range.

1.4 Construction and Operation of BLDC machine

Typical BLDC machine consists of the following parts

1. Stator which hosts of system of conductors.
2. Rotor where Permanent Magnets are mounted.
3. Rotor position sensor using Hall sensors.

1.4.1 Stator

The stator of a BLDC machine consists of windings wound over stacked steel laminations. The windings are distributed over the entire periphery and their ends are inter-connected to determine the number of poles. The number of windings determine the number of phases of the motor. The figure 1.2 represents the connection diagram of stator windings.

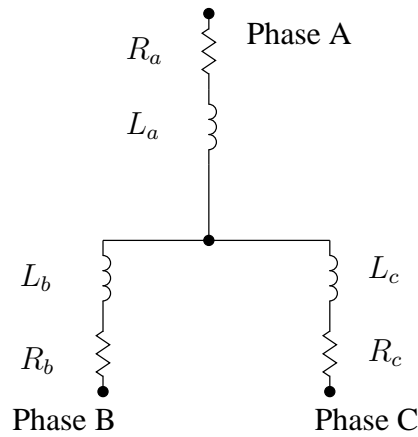


Figure 1.2: Connection diagram of Stator winding

1.4.2 Rotor

The rotor of a BLDC machine consists of permanent magnets either mounted on the surface or interior. Permanent magnets can be classified based on the flux density, relative permeability and other parameters. Ferrites are commonly used since they are available abundantly and less expensive though they possess less flux density. Rare earth magnets such as NdFeB, SmCo, AlNiCo which have high flux density but they are very expensive.

There are different placement of permanent magnets on the rotor and accordingly it is classified as shown in figure1.3, figure1.4 and figure1.5 respectively.

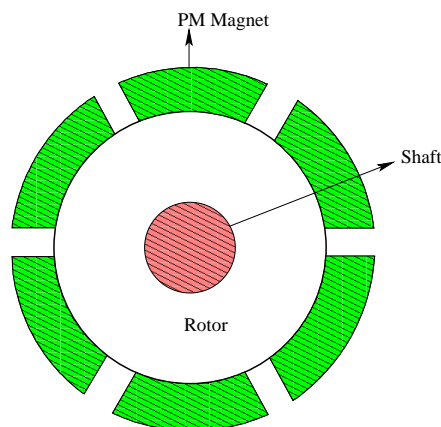


Figure 1.3: Surface-Mount Rotor BLDC

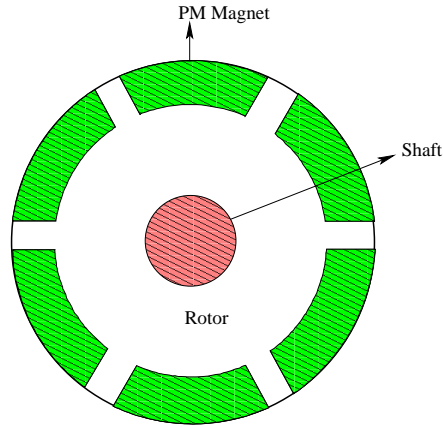


Figure 1.4: Inset Mount Rotor BLDC

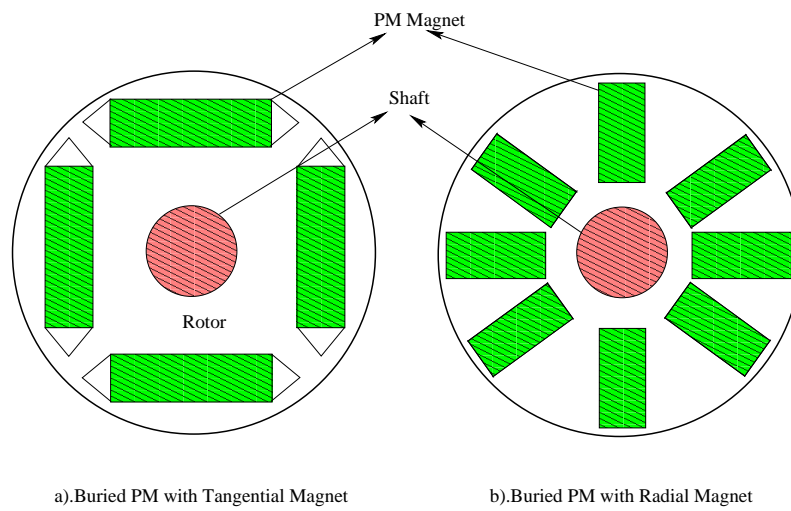


Figure 1.5: Buried PM Rotor BLDC

1.4.3 Hall sensors

The position of the rotor is determined by Hall sensors which are normally mounted on the stationary part. Hall sensors are placed 120° apart and six commutation sequences are achieved using possible combinations of three hall sensors. The hall sensor requires DC power source of 3 V to 36 V and sinks 15 mA of current with open-collector type output. The main drawback of using hall sensors is reduced immunity to electromagnetic interference and noises. The figure 1.6 shows the overall block diagram of operation of BLDC machine.

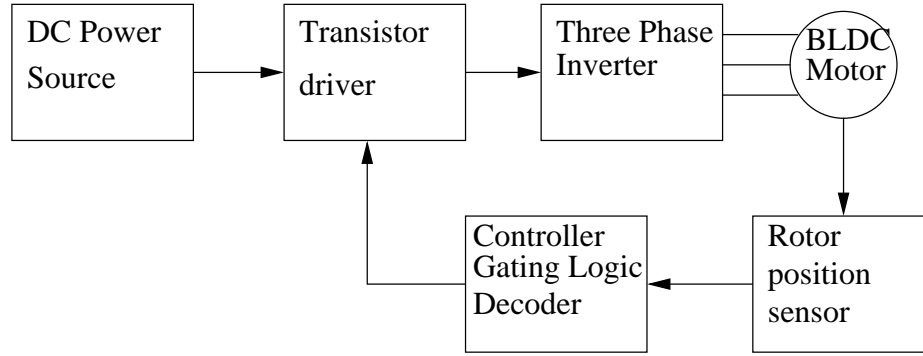


Figure 1.6: Operation of BLDC machine

1.4.4 Operation of BLDC motor

A BLDC machine with star-connected stator windings and two-pole rotor is considered for explanation. In order to obtain the rotation, stator coils have to be energized in a particular sequence and hence three phase inverter is connected. The gating pulses to the inverter switches are determined based on the position of the rotor. At any instant of time, only two phases will be conducting and third phase will be left open. The hall sensors are displaced 30° from the zero crossing of the respective back-emf.

With respect to DC bus ground, each leg mid-point voltage can take two values. Hence, the total number of switching states are eight. Of these, two combinations do not provide motor torque. This switching of the stator to build up rotation is called commutation. For three phase stator windings, there are six-step commutation^[4] as shown in table 1.1.

Table 1.1: Commutation Sequence based on Hall Sensor outputs

Rotor position	H_a	H_b	H_c	S1	S2	S3	S4	S5	S6	Phase to which full voltage is applied
0° - 60°	0	0	1	0	0	0	0	1	1	CB
60° - 120°	1	0	1	1	0	0	0	0	1	AB
120° - 180°	1	0	0	1	1	0	0	0	0	AC
180° - 240°	1	1	0	0	1	1	0	0	0	BC
240° - 300°	0	1	0	0	0	1	1	0	0	BA
300° - 360°	0	1	1	0	0	0	1	1	0	CA

The BLDC machine is similar to DC machine with respect to operation

except three phases are to be considered. The back-emf developed is a function of the position of the rotor. The torque of the motor is given by the product of phase current and back-emf of the corresponding phase and divided by the rotor speed. The following figure 1.7 depicts the back-emf and corresponding phase current in ideal case. The construction of stator and its winding arrangement will produce back-emf and corresponding phase current as shown in figure 1.9.

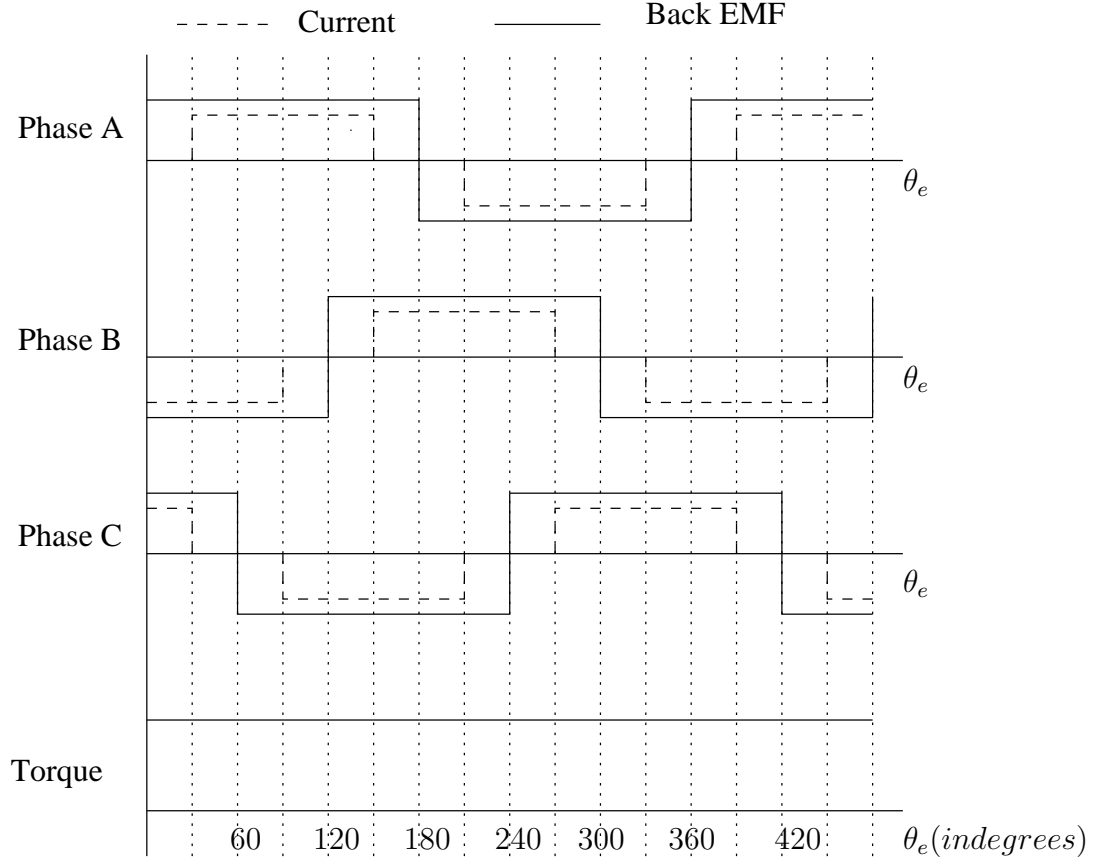


Figure 1.7: Ideal case waveforms Back-EMF and Phase current for 360°

The dynamic and steady state equations of BLDC machine are derived from the equivalent circuit as shown in figure 1.8.

$$v_a = R_a i_a + L_a \frac{di_a}{dt} + e_a \quad (1.1)$$

$$v_b = R_b i_b + L_b \frac{di_b}{dt} + e_b \quad (1.2)$$

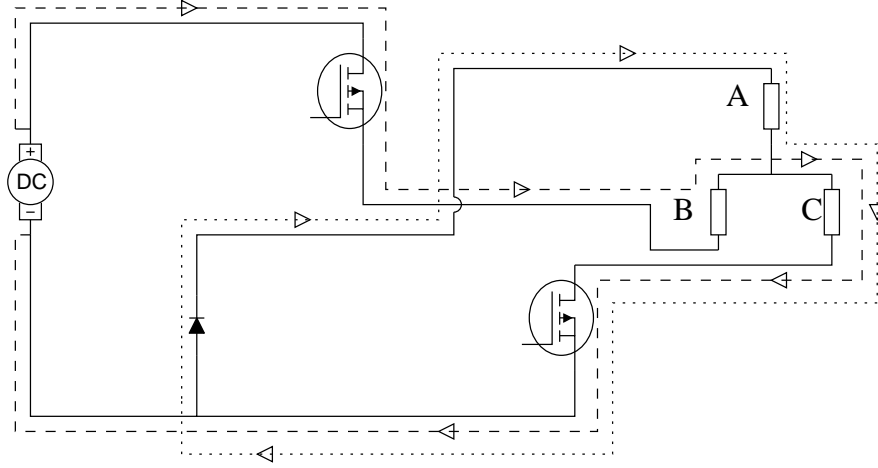


Figure 1.8: Equivalent circuit of BLDC machine when B and C phases are conducting and A phase freewheeling

$$v_c = R_c i_c + L_c \frac{di_c}{dt} + e_c \quad (1.3)$$

where,

v_a - instantaneous voltage of A - phase. Similarly v_b and v_c .

i_a - instantaneous phase current of A-phase. Similarly i_b and i_c .

R_a, R_b, R_c - resistances of A,B and C phase. Normally $R = R_a = R_b = R_c$.

L_a, L_b, L_c - inductances of A,B and C phase. Normally $L = L_a = L_b = L_c$.

e_a - back-emf developed in A-phase. Similarly e_b and e_c .

Since the machine is star-connected,

$$i_a + i_b + i_c = 0 \quad (1.4)$$

For the equivalent circuit shown in figure1.8

the corresponding electrical equations

$$L \frac{di_a}{dt} = -(2E - V_{dc})/3 \quad (1.5)$$

$$L \frac{di_b}{dt} = (2E - V_{dc})/3 \quad (1.6)$$

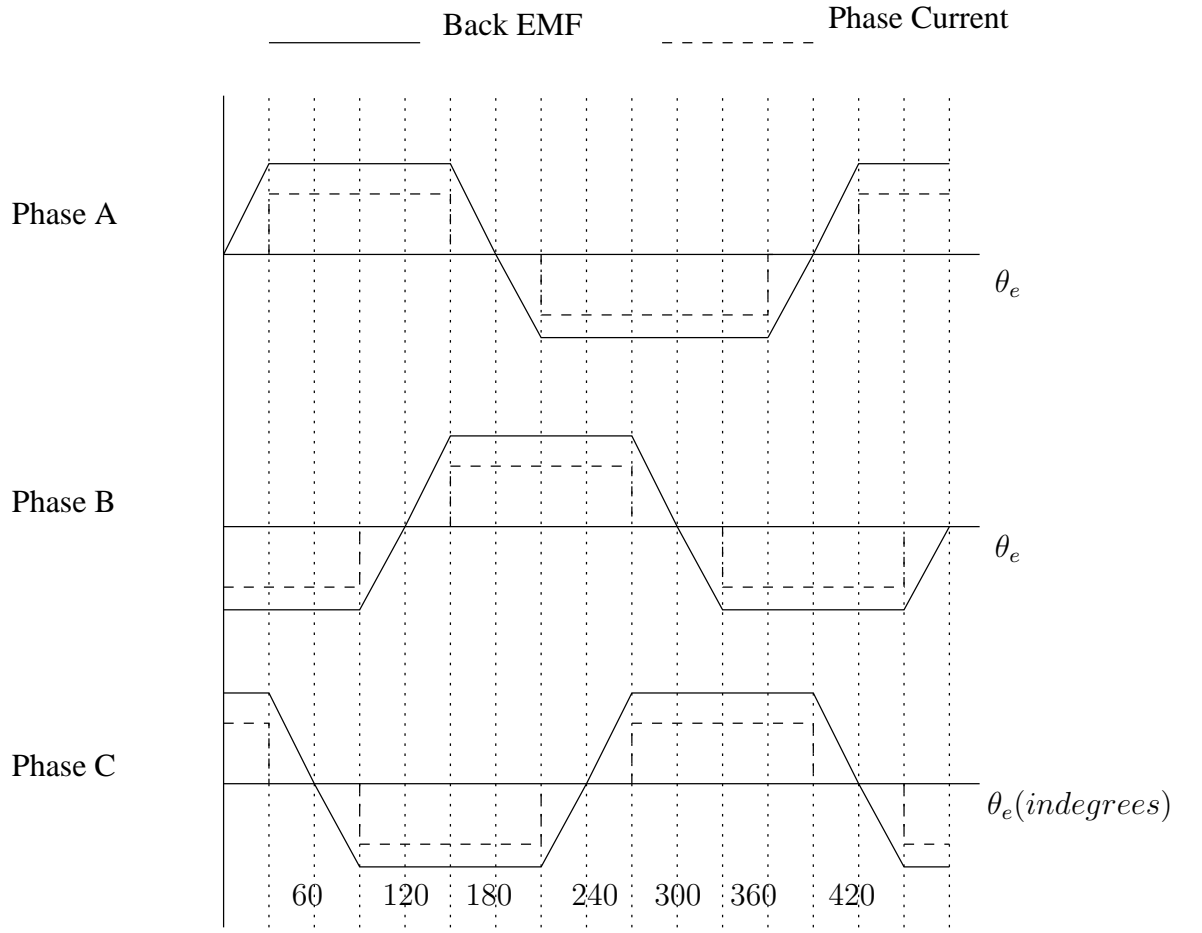


Figure 1.9: Back-EMF and Phase current for 360°

$$L \frac{di_c}{dt} = (4E - V_{dc})/3 \quad (1.7)$$

Back-emf equations are given as

$$e_a = K_e(\theta)\omega \quad (1.8)$$

$$e_b = K_e(\theta - 2\pi/3)\omega \quad (1.9)$$

$$e_c = K_e(\theta - 4\pi/3)\omega \quad (1.10)$$

where,

K_e = back-emf constant

θ = Rotor position

ω = angular velocity of the rotor

Back-EMF constant is a function of rotor position and represented for 360° for Phase A

$$K_e(\theta) = \left(\frac{6E}{\pi}\right) * \theta \text{ for } 0 \leq \theta \leq 30^\circ$$

$$K_e(\theta) = E \text{ for } 30^\circ \leq \theta \leq 150^\circ$$

$$K_e(\theta) = -\left(\frac{6E}{\pi}\right) * \theta + 6E \text{ for } 150^\circ \leq \theta \leq 210^\circ$$

$$K_e(\theta) = -E \text{ for } 210^\circ \leq \theta \leq 330^\circ$$

$$K_e(\theta) = \left(\frac{6E}{\pi}\right) * \theta - 12E \text{ for } 330^\circ \leq \theta \leq 360^\circ$$

Similarly for Phase B and Phase C except phase shifted by 120° and 240°

Electromagnetic Torque equation

$$T_e = K_t(\theta)i_a + K_t(\theta - 2\pi/3)i_b + K_t(\theta - 4\pi/3)i_c \quad (1.11)$$

Where, K_t = Torque constant

Mechanical Equations:

$$T_e = T_l + J\frac{d\omega}{dt} + B\omega \quad (1.12)$$

where, T_l = Load Torque

J = Rotor inertia

B = Damping Co-efficient

Transfer function for Electrical System under steady state condition

$$V_a(s) = (R + sL)I_a(s) \quad (1.13)$$

$$\frac{I_a(s)}{V_a(s)} = \frac{1}{R + sL} \quad (1.14)$$

where, $\tau_{elec} = \frac{L}{R}$

Transfer function for Mechanical System

$$K_t I_a(s) = (sJ + B)\omega(s) \quad (1.15)$$

$$\frac{\omega(s)}{I_a(s)} = \frac{K_t}{sJ + B} \quad (1.16)$$

where, $\tau_{mech} = \frac{J}{B}$

Transfer function for combined system

$$\frac{\omega(s)}{V(s)} = \frac{\omega(s)}{I(s)} * \frac{I(s)}{V(s)} \quad (1.17)$$

$$\frac{\omega(s)}{V(s)} = \frac{K_t}{sJ + B} * \frac{1}{R + sL} \quad (1.18)$$

which gives electromechanical time constant

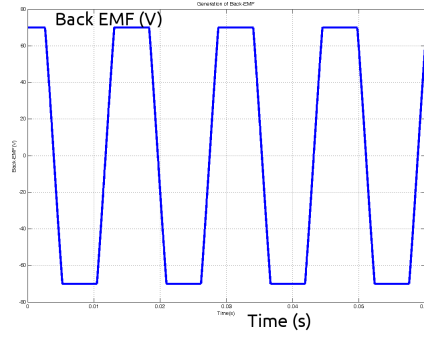
$$\tau_{em} = \frac{JR_a}{(K_t)^2}$$

1.5 Theoretical Understanding of BLDC machine model

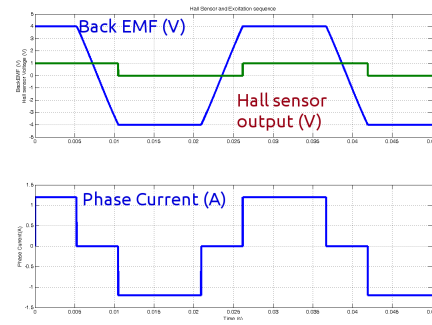
Initially BLDC machine with mechanical input is given and made the machine to operate as generator. The back-emf are measured and found that trapezoidal back-emf as shown in figure1.10a. It also requires mechanism to sense the position of rotor. The hall-sensor can be used to sense the zero crossing of back-emf by giving high pulses. Three hall sensors are placed 120° apart from each other. The sequence of excitation based on hall sensor outputs should produce constant power, which requires displacement of hall sensors by 30° with respect to zero crossing of the back-emf as shown in figure1.10b. The Phase current will have duration of 120° and of quasi-square shape. The gate pulses to the machine for the phase A is given in figure1.10c.

Observations:

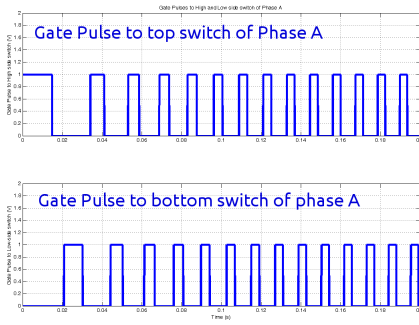
From the figure 1.10a, Suppose a speed input of ω rad/s is given to the BLDC machine



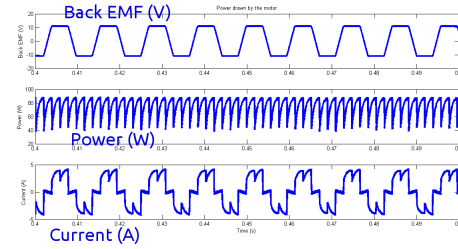
(a) BLDC run with mechanical input



(b) BLDC machine with hall sensor based excitation



(c) Gate Pulses given to Phase A



(d) Power developed in the motor

Figure 1.10: Waveforms describing BLDC operation

and back-emf developed is given by

$$E_b = K_b * \omega_m \quad (1.19)$$

From the figure 1.10b, Hall sensor position inside the machine is at 30° with respect to give zero crossing of back-emf and excitation provided to corresponding phase where back-emf is constant so that constant power is developed which is shown in figure 1.10d.

The implementation of chopping in gate pulses provides us control over the output average voltage of the inverter. There are two types of chopping such as Hard chopping and Soft Chopping. Hard Chopping means both high side switches and low side switches are triggered with PWM pulses as shown in figure 1.11a. Both switches are ON or there will be instants where both switches are OFF. Soft chopping is the method where high side switch is kept ON and low side switch is chopped. Soft Chopping has the advantage of less stress experienced by the chopped switch in comparison with hard

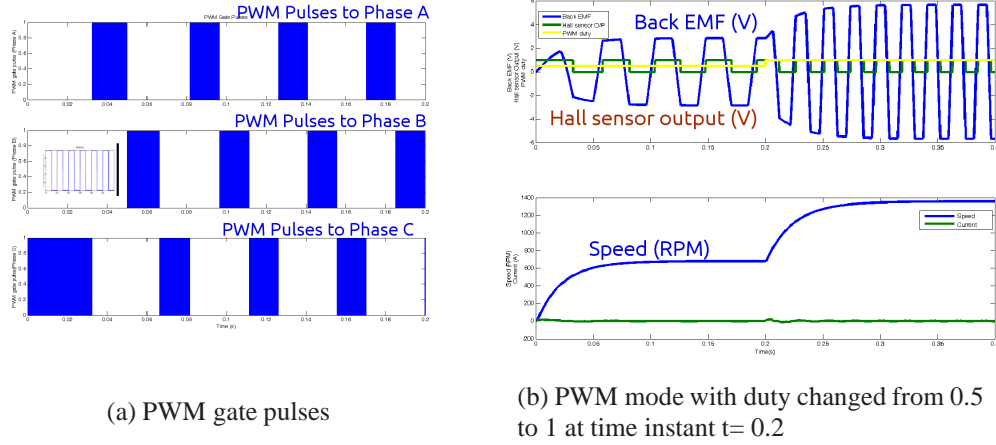


Figure 1.11: Waveforms of BLDC operation in PWM mode

chopping. From 1.11b, PWM with duty changed from 0.5 to 1 at $t = 0.2$ s, where speed is doubled with time constant.

1.6 Organization of Project Report

Chapter 2 deals with the controller design for the BLDC machine. Also comparison of simulation results (both open loop and closed loop) with the theoretical results has been presented.

Chapter 3 deals with the hardware implementation of the inverter circuit and controller circuit and their corresponding experimental results.

Chapter 4 presents the summary and scope for future development.

CHAPTER 2

Design of Controller and Simulation Results

2.1 Simulation Results of BLDC machine in Open loop

The specifications and machine parameters used for simulation is given in Appendix A.

In the open loop, the power switches in the inverter are triggered with fixed duty. The gate pulses to the power switches are derived from six possible combinations of three hall sensor outputs which are displaced by 120° . This mode of operation is known as “Sensored Operation” of BLDC machine.

Otherwise, the gate pulses can also be derived from the zero crossing of Back-emf signals thereby eliminating the need of hall sensors. This method of operation is called “Sensorless operation” of BLDC motor.

2.1.1 Sensored Operation in Open loop

The position of the rotor is sensed by placing the hall sensor in the stationary part or in the stator itself^[2]. The hall sensor requires DC power source and pull-up resistor in the output since its open-collector output. A BLDC machine with parameters mentioned in Appendix A is simulated in MATLAB and the corresponding machine quantities are plotted. The BLDC machine is taken from MATLAB library which will have internal signal conditioning subsystems so that the measured quantities are smooth. Also, the power electronic devices used are ideal and did not have snubber circuits. The practical implementation of these devices should be taken care of and will be discussed in the next chapter. The placement of Hall sensor inside the machine pose critical effect on the performance of the machine. Normally, the hall sensors are positioned 30° after the zero-crossing of the back-emf. Depending upon the hall-sensor outputs, the commu-

tation logic is derived in MATLAB function file which will be included in the path of SIMULINK file where machine is used for simulation.

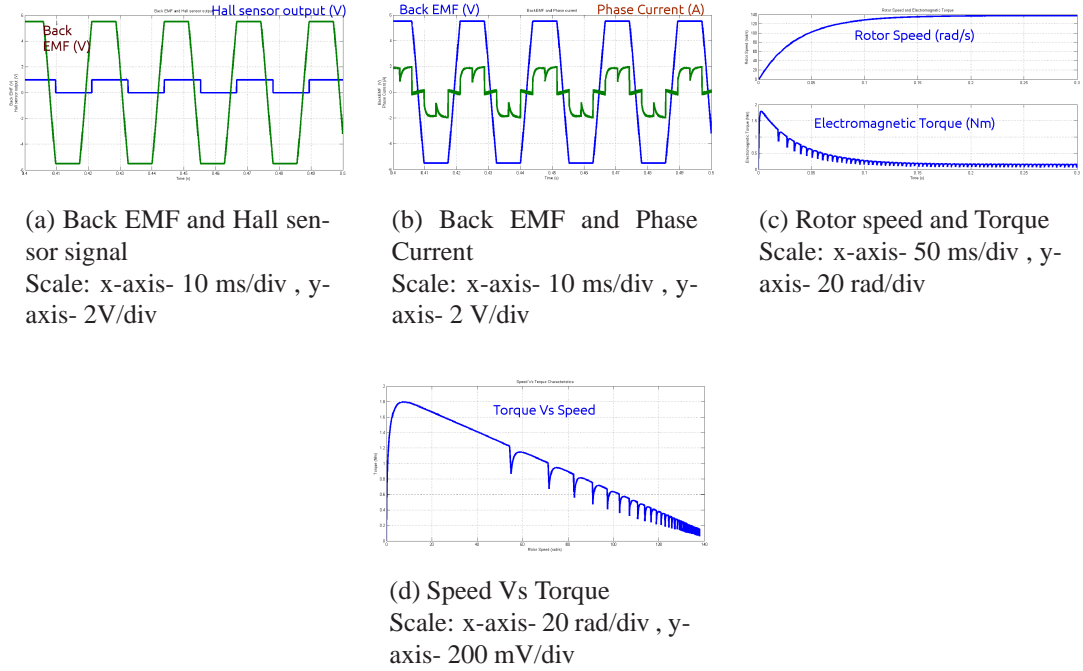


Figure 2.1: Sensored Operation of BLDC in open loop

Observation:

All the above simulations are done with $V_{dc} = 24$ V and $T_l = 0$ Nm and observed that From 2.1a, Back-EMF and Corresponding Hall sensor output are plotted and 30° displacement between hall sensor and back-emf.

From 2.1b, Phase Back-EMF and corresponding phase current are plotted. Phase current = 0.3 A is drawn under this condition.

From 2.1c, Rotor speed attains the final speed in less than 0.15 s since initial T_e is large due to large I_a .

From 2.1d, Initially torque is high due to high starting current and then switching ripple is reflected in the torque ripple.

When the machine is loaded in open-loop condition using sensed control, the speed of the machine dips and the slope of the deceleration depends upon the rate at which load is applied.

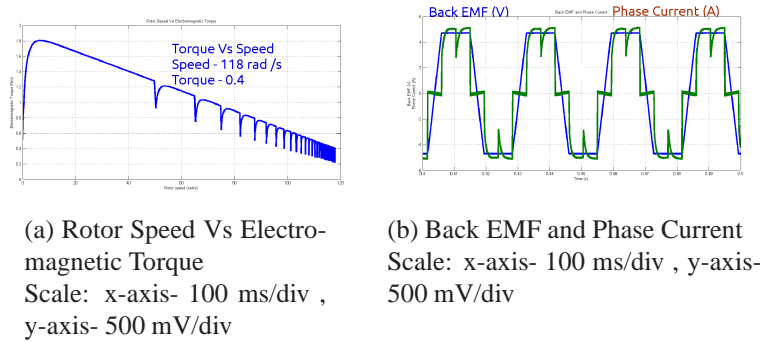


Figure 2.2: Sensored Operation of BLDC in open loop under loaded condition

Observation:

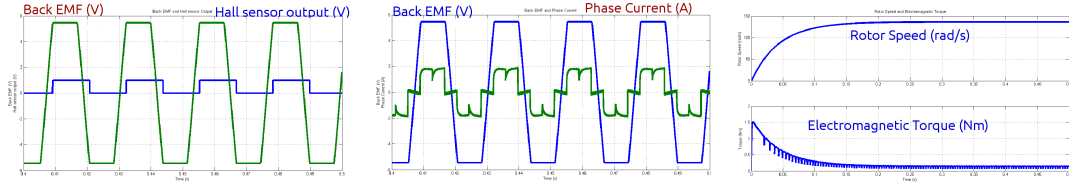
From the Figure 2.2a and 2.2b, it is observed the rotor speed is decreased to 120 rad/s and the phase current is increased to 5 A. When the brake torque is more than the electromagnetic torque, the motor speed will reach zero and will accelerate in the reverse direction.

2.1.2 Sensorless Operation in Open loop

In applications where cost-effective BLDC machines have to be developed, then hall sensors are eliminated. The position of the rotor will be determined indirectly. In the past, there are lot of techniques proposed for sensing rotor position. Among these techniques, back-emf signals are mostly used for sensing rotor position from zero-crossing detection. The major drawback of Sensorless operation is that when motor operates at low speed and at starting, the back-emf will be low and very difficult to find zero crossing. So, we have to use start-up algorithm where random gate pulse triggering up to a particular speed and then zero crossing detection method is employed.

Table 2.1: Comparison of sensored and sensorless operation

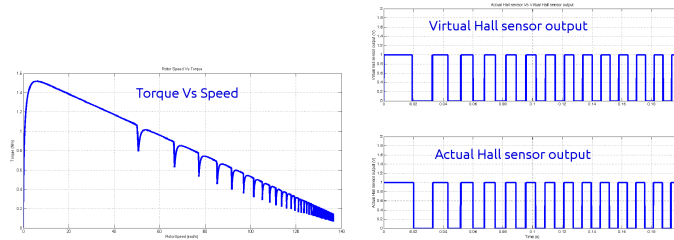
S.No	Features	Sensored control	Sensorless control
1	Implementation Cost	High	Low
2	Accuracy of position sensing	High at all RPM	Less at starting and low RPM
3	Output	Pull-up resistor is required	Requires Phase Delay of 30°



(a) Back EMF and Hall sensor signal
Scale: x-axis- 10 ms/div , y-axis- 2 V/div

(b) Back EMF and Phase Current
Scale: x-axis- 10 ms/div , y-axis- 2 V/div

(c) Rotor speed and Torque
Scale: x-axis- 50 ms/div , y1-axis- 50 rad/div y2-axis - 500 mN/div



(d) Speed Vs Torque
Scale: x-axis- 20 rad/div , y-axis- 200 mN/div

(e) Actual Vs Virtual Hall sensor signals
Scale: x-axis- 10 ms/div , y-axis- 200 mV/div

Figure 2.3: Sensorless Operation of BLDC in open loop

Observation:

From the Figure 2.3a, the zero crossing of back-emf and hall sensor signals for phase A is having 30° displacement.

From the Figure 2.3b, the phase current is of quasi-square wave shape and back-emf for phase A with respect to phase current is plotted.

From the Figure 2.3c, the mechanical characteristics of motor shows that no-load speed is 147 rad/sec and torque is 0.1 Nm

From the Figure 2.3d, the initial torque of the motor is 1.8 Nm and then torque ripple at switching instants.

From the Figure 2.3e, the actual and virtual hall sensors are similar.

It is observed that sensed mode and sensorless mode are giving the similar output.

2.2 Design of Controller

There are applications where desired operation is required and this objective is achieved through the implementation of suitable control algorithm. In fan applications, where constant torque is developed and in turn constant speed can be achieved through the speed controller. In applications where load is not constant, current loop is implemented to reduce torque ripple. There are three commonly used techniques for achieving the control in BLDC machine.

1. DC Link Voltage control
2. Pulse Width Modulation control
3. Hysteresis control

2.2.1 DC Link Voltage Control

The BLDC machine supply is fed from the inverter, which in turn provided by conventional AC supply through phase controlled rectifier. By controlling the firing angle, the DC link voltage is controlled and thereby controlling the machine input power. This method provides two conversion AC to DC and again DC to Square pulsed output. In each stage, the use of power electronic devices contribute to power loss and thus, limiting the range of operation of the circuit.

2.2.2 Pulse Width Modulation Control

The Pulse Width Modulation technique is a constant frequency, variable on-time. It is easy to design filter and select the cut-off frequency as frequency of operation is constant. Pulse width modulation further can be realized using different sub-techniques. The carrier signal should be generated which determines the switching frequency. The selection of switching frequency is a compromise solution depending upon applications. For high frequency switching, the switching loss will be comparable and reduce the efficiency of the converter. For low frequency switching, the controller bandwidth is limited. Electromagnetic Interference and Noises will contribute and affect the modulation signal.

2.2.3 Hysteresis Control

This is the simplest algorithm through which control is achieved. The hysteresis band should be selected and band width should be chosen accordingly. EMI and Noise issues will not be there but frequency of operation is not constant and difficult to design the filter^[3].

The complete controller block diagram is as shown in figure 2.4

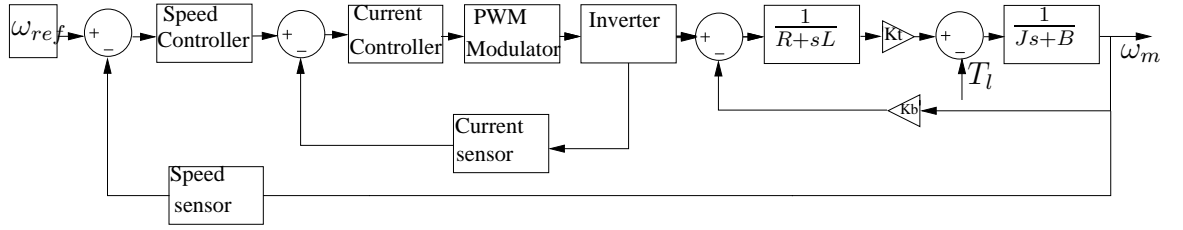


Figure 2.4: Block Diagram of Complete Controller Design

2.2.4 Machine parameters

Resistance per phase $R = 0.15369\Omega$

Inductance per phase $L = 0.00016H$

Effective Resistance $R_a = 2 * R = 0.30738\Omega$

Effective Inductance $L_a = 2 * L = 0.00032H$

Electrical Time Constant $\tau_{elec} = L_a / R_a = 1.04ms$

Rotor Inertia $J = 5e-4 \text{ kg-m}^2$

Friction Co-efficient $B = 1e-3$

Mechanical Time Constant $\tau_{mech} = J/B = 0.1s$

Switching Frequency $f_s = 10 \text{ kHz}$

Back-EMF constant $K = 0.04 \text{ V/rad/s}$

Effective Back-EMF constant $K_b = 2 * K = 0.08 \text{ V/rad/sec}$

Inverter Gain $K_I = 24$

Inverter delay $\tau_I = 1/(2*f_s) = 0.5e-4$

Current Sensor gain $K_2 = 0.1$

Current Sensor delay $\tau_2 = 3.183e-5$

2.2.5 Design of Current Controller

The generic block diagram representing the motor in mathematical model using transfer functions as shown in figure 2.5.

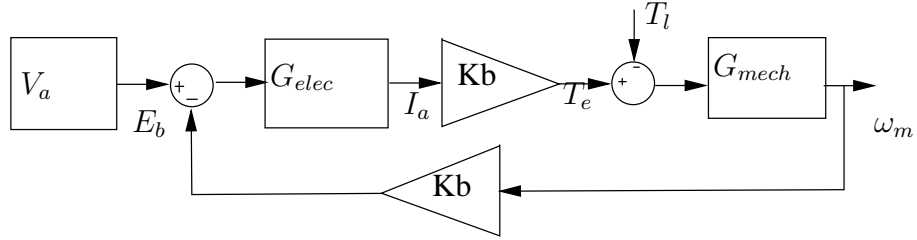


Figure 2.5: Plant structure including electrical and mechanical

where,

G_{elec} = Electrical system Transfer function

G_{mech} = Mechanical system Transfer function

The derivation of G_{elec} is given as follows

$$V_a - E_b = I_a(R_a(1+s\tau_{elec}))$$

$$\frac{I_a(s)}{V_a(s)} = \frac{1}{R_a(1 + s\tau_{elec}) + \frac{Kb^2}{B(1+s\tau_{mech})}} \quad (2.1)$$

$$\frac{I_a(s)}{V_a(s)} = \frac{\frac{1+s\tau_{mech}}{R_a}}{s^2\tau_{mech}\tau_{elec} + s(\tau_{elec} + \tau_{mech}) + (1 + \frac{Kb^2}{BR_a})} \quad (2.2)$$

After doing first order approximation

$$\frac{I_a(s)}{V_a(s)} = \frac{1}{R_a(1 + s\tau_{elec})} \quad (2.3)$$

The bode plot of the plant transfer function is given by

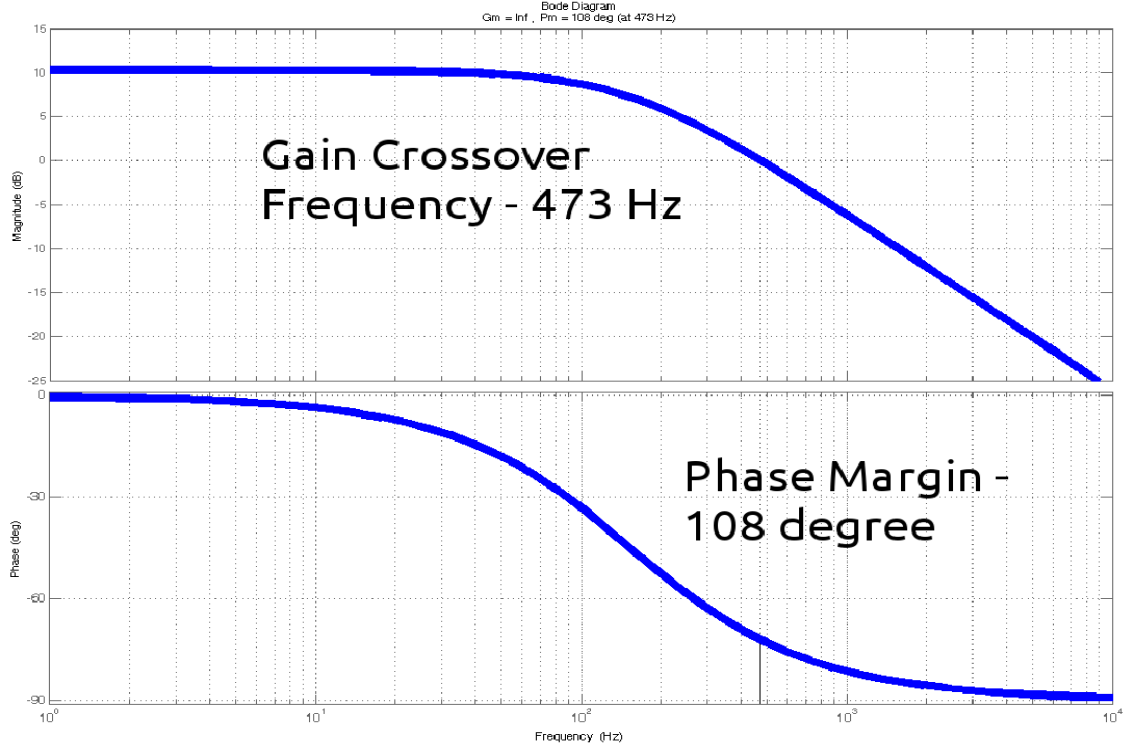


Figure 2.6: Bode Diagram for Plant transfer function

Observation:

From the plot 2.6, it is found that the bandwidth of inner loop is 473 Hz. In order to improve the bandwidth of the inner loop, PI controller is added so that initial gain improved by appropriately selecting K_p and steady state error is nullified by selecting K_I .

Implementation of Current Controller to achieve constant torque and reduced overshoot during sudden loading conditions. Proportional - Integral Controller is chosen with appropriate K_p and K_I values. The effect of inverter delay and current sensor delay are also considered. The block diagram representing the current controller is represented as shown in figure 2.7.

$$\frac{I_{act}(s)}{I_{ref}(s)} = \frac{\frac{K_c(1+s\tau_c)K_I}{V_m R_a(1+s\tau_{elec})(1+s\tau_I)s\tau_c}}{1 + \frac{K_c(1+s\tau_c)K_I K_2}{V_m R_a(1+s\tau_{elec})(1+s\tau_I)(1+s\tau_2)s\tau_c}} \quad (2.4)$$

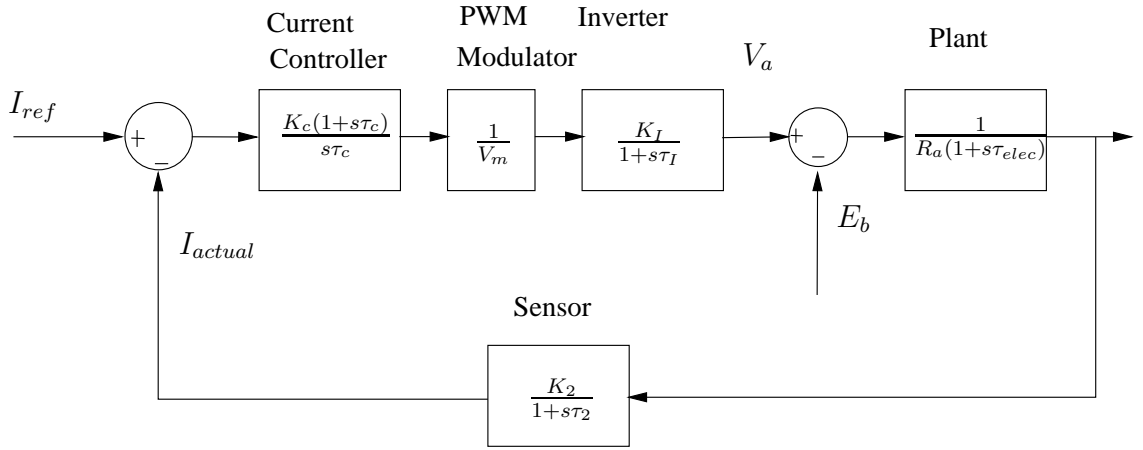


Figure 2.7: Implementation of Current Controller

Here, $V_m = 1$

The bandwidth of the Current loop is chosen as 2 kHz. Inverter delay is assumed to be half of the switching frequency and current sensor delay is also negligible.

The loop gain of the current controller is taken and compared with desired bandwidth to get K_p value.

Assume, $\tau_c = \tau_{elec}$

$$\frac{1}{s\tau_{desired}} = \frac{K_c(1+s\tau_c)K_I K_2}{R_a s\tau_c(1+s\tau_I)(1+s\tau_{elec})(1+s\tau_2)} \quad (2.5)$$

From the above equation,

$$K_c = 0.1676$$

$$\tau_c = 1.04\text{ms}$$

which gives, $K_p = 0.1676$ and $K_I = 167.6$

The bode diagram of the compensated loop gain I_{actual} / I_{ref} is as shown in figure 2.8.

Observation:

From the plot 2.8, the bandwidth of compensated loop is 1.76 kHz. As per Thumb rule, The Gain Margin should be above 6 dB and Phase Margin should be above 50° . In our

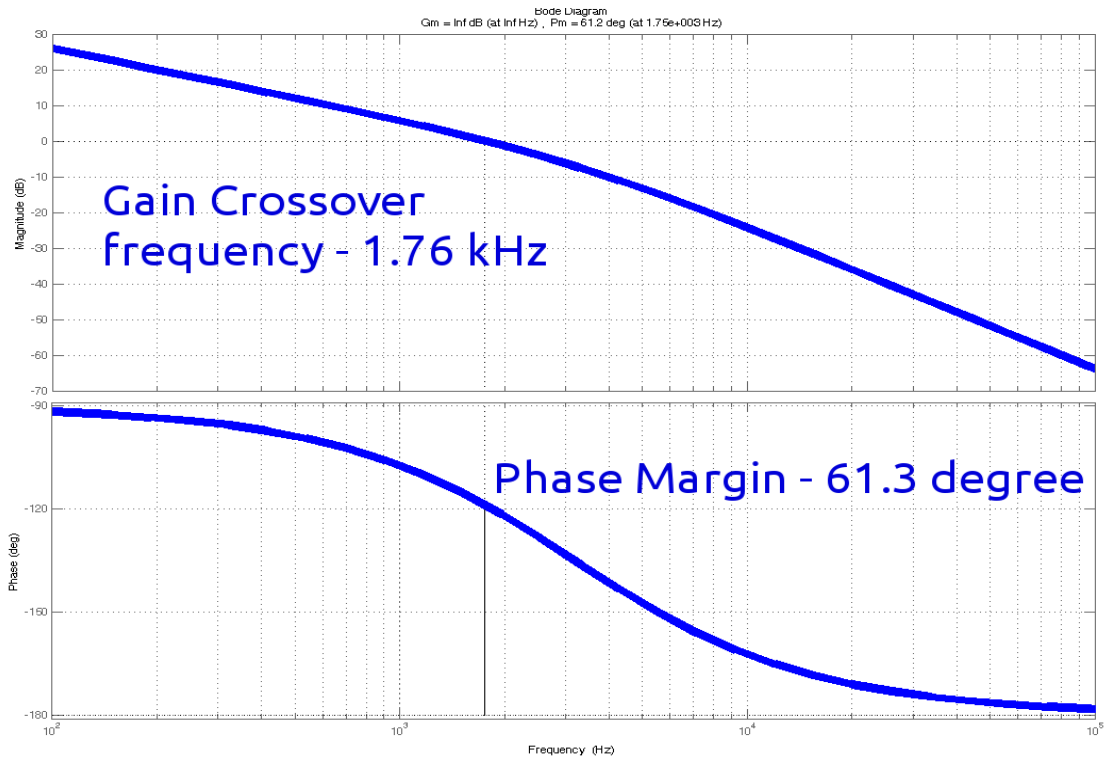


Figure 2.8: Bode Diagram for Compensated Loop gain function of inner current loop

condition, Gain Margin is infinite and Phase Margin is 61.3° .

The DC Bus current is also a representation of motor current since at any instant of time, only two phases are conducting. One top switch and one bottom switch will conduct. Hence, Current sense resistor will be kept in the return path of the DC bus in order to avoid the grounding and noise problems. The Value of current sense resistor is chosen as a matter of compromise. If higher value of current sense resistor is selected, high accuracy and can be used over entire voltage range. If low value of resistance is selected, low voltage drop and hence low power loss.

The step response plot of the I_{actual} / I_{ref} closed loop is as shown in figure 2.9.

Observation:

From the figure 2.9, the settling time of the current is found to be 1.04 ms, which is equivalent to electrical time constant.

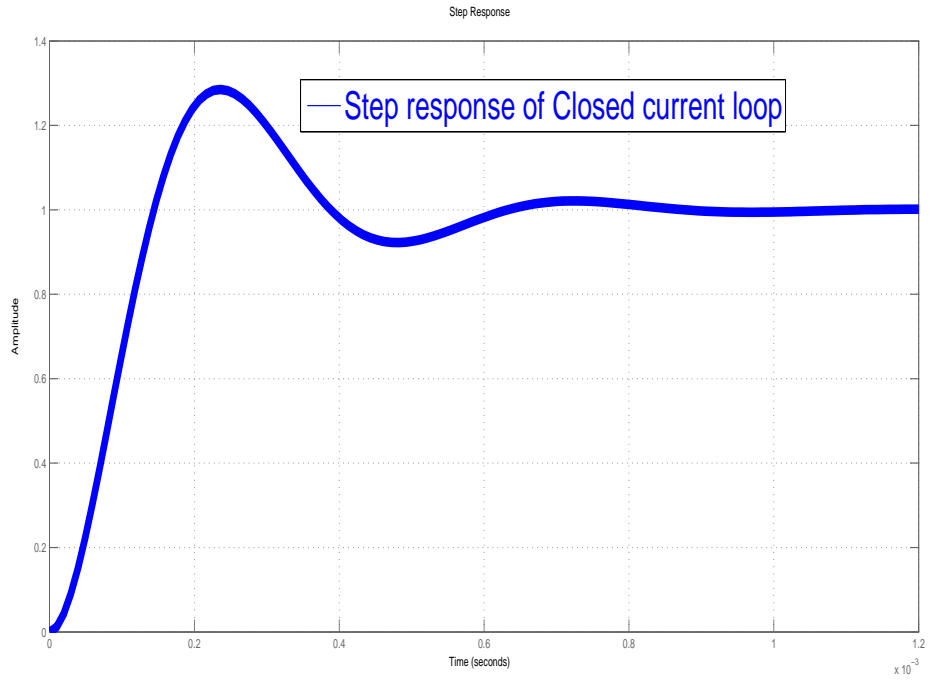


Figure 2.9: Step response of inner current loop

2.2.6 Design of Speed Controller

The block diagram representing the speed controller as shown in figure 2.10.

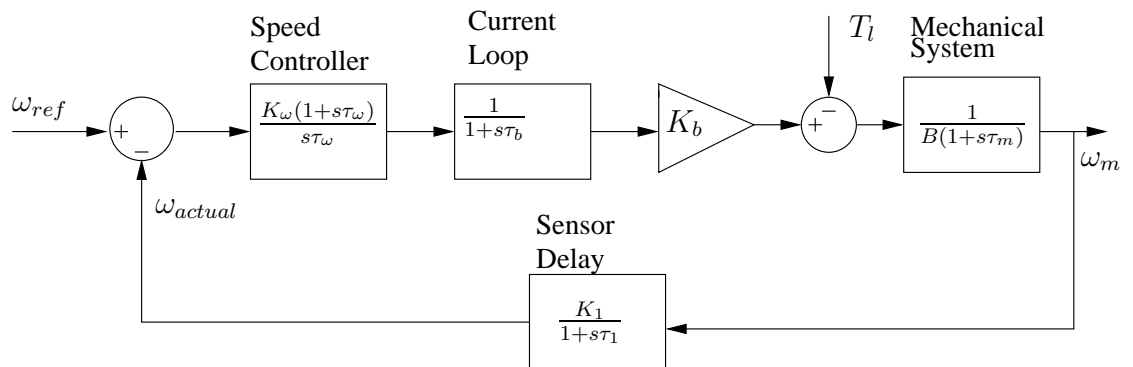


Figure 2.10: Implementation of Speed Controller

The mechanical system of the machine without implementing any control loop has system characteristics as shown in figure 2.11.

Observation:

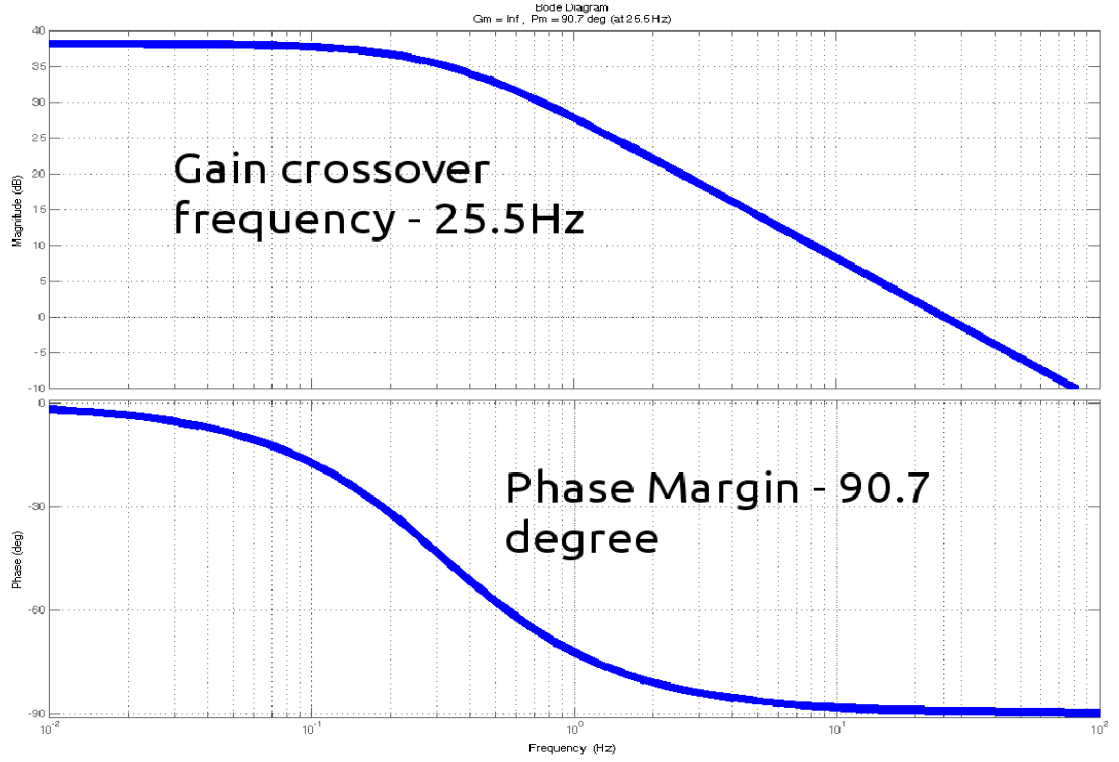


Figure 2.11: Bode Diagram for Mechanical system transfer function

From the plot 2.11, the bandwidth of the mechanical system is found to be 25 Hz.

The outer speed control loop, which have bandwidth lesser than the inner current loop, is built using Proportional and Integral controller. The effect of sensor delay and inner current loop are also taken into consideration.

$$\frac{\omega_{actual}}{\omega_{ref}} = \frac{\frac{K_{\omega}(1+s\tau_{\omega})K_b}{B(1+s\tau_{mech})(1+s\tau_b)s\tau_{\omega}}}{1 + \frac{K_{\omega}(1+s\tau_{\omega})K_bK_1}{B(1+s\tau_{mech})(1+s\tau_b)(1+s\tau_1)s\tau_{\omega}}} \quad (2.6)$$

If friction co-efficient is not known, then we can design the controller using a technique known as “Symmetrical Optimization”. Select the speed loop bandwidth such that corner frequency is at geometric mean of product of τ_c and τ_{ω}

The bandwidth of the speed loop is chosen as 500 Hz. The Compensated loop gain for the speed control loop is compared with desired bandwidth and we obtain K_p and K_I values.

Compensated Loop gain is given by

$$GHs = \frac{K_\omega(1 + s\tau_\omega)K_1R_a}{KbK_2(s\tau_{em})(1 + s(2\sigma))(1 + s\tau_1)} \quad (2.7)$$

where, $\sigma = \tau_b + \tau_2$

After doing first order approximation

$$GHs = \frac{K_\omega(1 + s\tau_\omega)K_1R_a}{KbK_2(s\tau_{em})(1 + s(2\sigma + \tau_1))} \quad (2.8)$$

where, $\delta = \tau_1 + 2\sigma$

Assume $\tau_\omega = 4 * \delta$, Select K_ω such that corner frequency $\omega_c = \frac{1}{\sqrt{\tau_\omega\delta}}$. Hence, $\omega_c = \frac{1}{2\delta}$

$$\tau_\omega = 4 * (500 * 10^{-6})$$

Electromechanical time constant $\tau_{em} = \frac{\tau_m * B * R_a}{Kb}$

$$K_\omega = (0.5 * Kb * \tau_{em}) / (R_a * 500 * 10^{-6})$$

$$\frac{1}{s\tau_{\omega(des)}} = \frac{K_\omega(1 + s\tau_\omega)K_bK_1}{Bs\tau_\omega(1 + s\tau_b)(1 + s\tau_{mech})(1 + s\tau_1)} \quad (2.9)$$

From the above equation,

$$K_\omega = 6.25, \tau_\omega = 2\text{ms which gives } K_p = 6.25 \text{ and } K_I = 3125$$

The bode diagram of the compensated loop gain $\omega_{actual} / \omega_{ref}$ is as shown in figure 2.12.

Observation:

From the plot 2.12,

the bandwidth of the outer loop is 176 Hz which is 1/10th of inner loop. The above condition is the ideal condition of obtaining the proportion of outer loop bandwidth to the inner loop bandwidth. The worst condition is that $\tau_\omega = 3 \tau_c$ This is achieved by

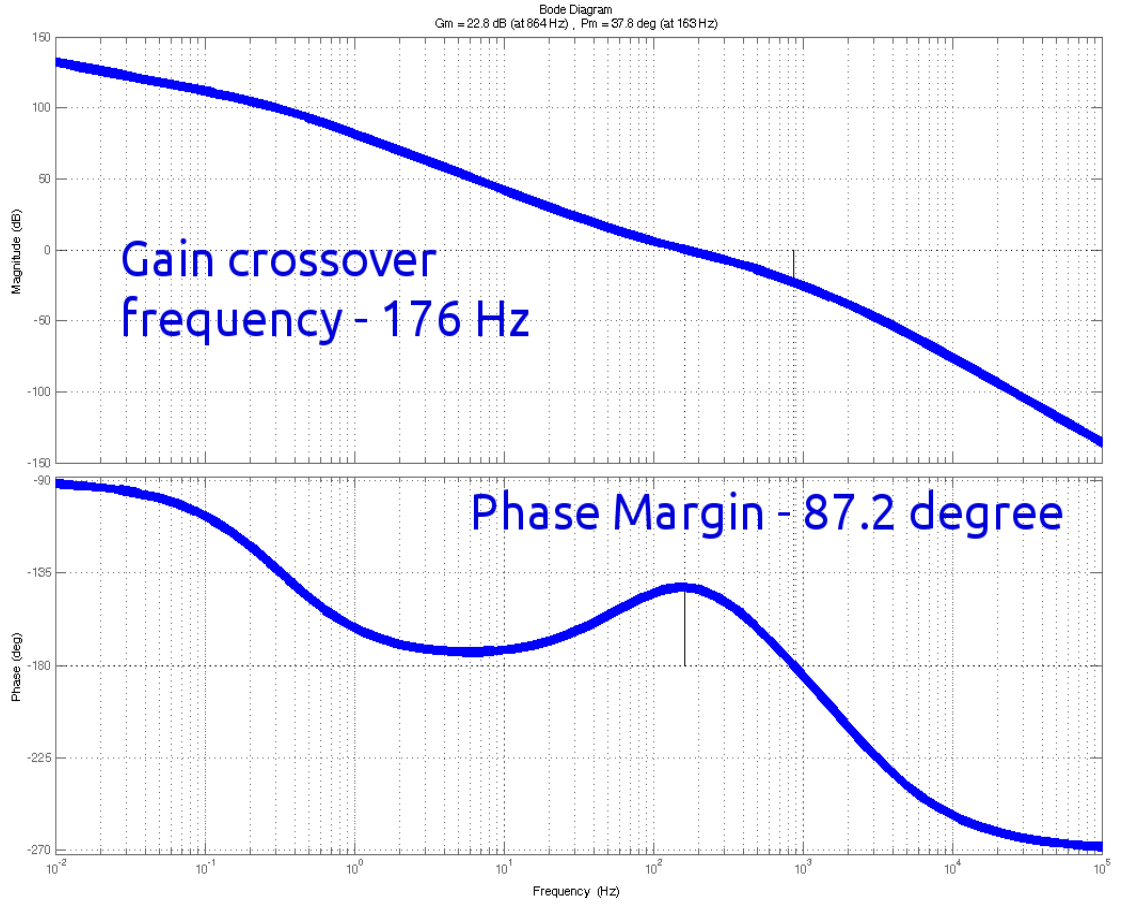


Figure 2.12: Bode Diagram for Compensated Loop gain function of outer speed loop

following mathematical computations using symmetric optimization.

The step response plot of the $\omega_{actual} / \omega_{ref}$ closed loop is as shown in figure 2.13.

Observation:

From the plot 2.13, the settling time for the speed to track the reference speed is around 10ms.

2.3 Simulation Results of BLDC machine in Closed loop

The BLDC machine model from MATLAB library with our machine parameters is selected and two loop control methodology is implemented with inner current loop and outer speed loop. The three phase inverter is built using MOSFETs and DC bus Capacitance is placed in parallel with power source. Pulse width modulation technique is used to control the duty of the gate pulses to the power switches thereby

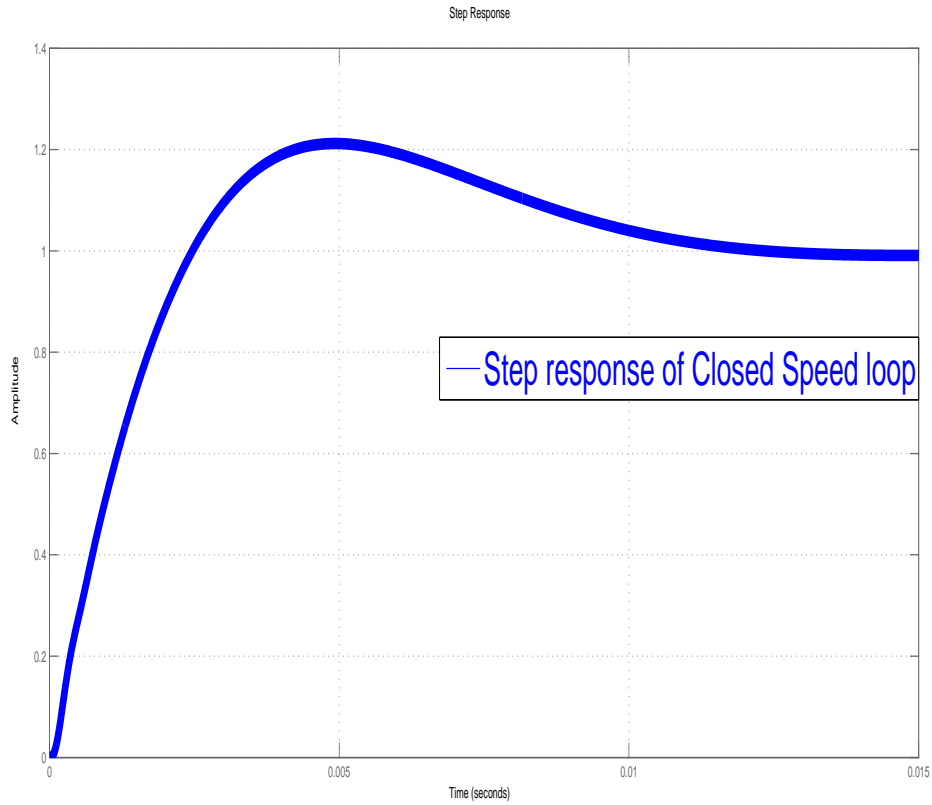


Figure 2.13: Step response of outer speed loop

controlling the speed.

Reference speed for the machine is given in step of 104.72 rad/s and $T_l = 0.1$ Nm at time $t = 1$ s. Simulation results are plotted and presented below.

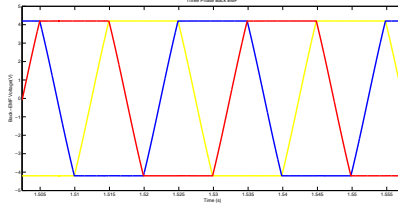
Observation:

From the figure2.14a, Three phase back-EMFs are measured with $V_{dc} = 24$ V and $T_l = 0.1$ Nm. The signal conditioning circuit inside the machine model gives smooth wave-forms of the back-emf.

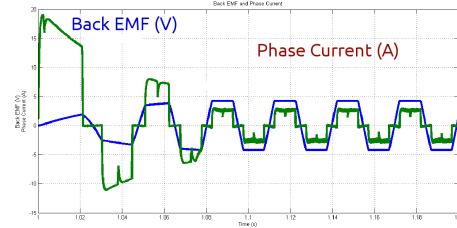
From the figure2.14b, Phase current will shoot-up at the instant of providing the reference speed and then settled under steady state value of 0.96 A.

From the figure2.14c, Electromagnetic Torque will increase proportionally to phase current and then settled under steady state value of 0.2 Nm since it has to overcome frictional torque.

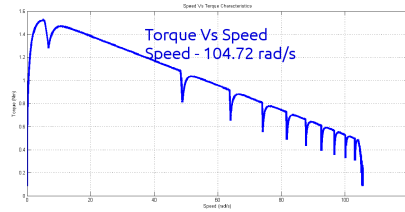
From the figure2.14d, Actual speed follows the reference speed and got settled at $t = 45$



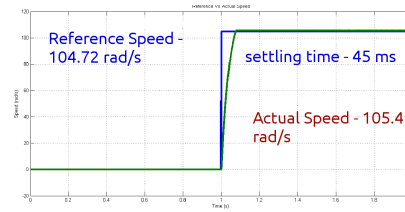
(a) Three Phase Back EMF
Scale: x-axis- 5 ms/div , y-axis- 1 V/div



(b) Back EMF and Motor Phase current
Scale: x-axis- 20 ms/div , y-axis- 5 V/div



(c) Rotor Speed Vs Electromagnetic Torque
Scale: x-axis- 20 rad/div , y-axis- 200 mN/div



(d) Reference Vs Actual Speed
Scale: x-axis- 200 ms/div , y-axis- 20 rad/div

Figure 2.14: Sensored Operation of BLDC in Closed loop with $V_{dc} = 12$ V and $T_l = 0.1$ Nm

ms.

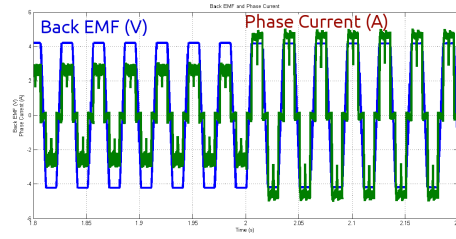
When the machine is loaded with load torque = 0.26Nm at time $t = 2$ s and the machine response to the step increase in the load is plotted.

From the figure2.15a, the phase current will increase by step at time $t = 2$ s and got settled at value 4.5 A.

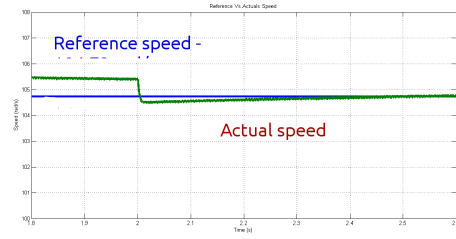
From the figure2.15b, There will be slight dip in the speed at the instant of load torque step increase and then speed will regulate towards the reference speed.

From the figure2.15c, the torque will increase by step at time $t = 2$ s and got settled at value of torque 0.36 Nm.

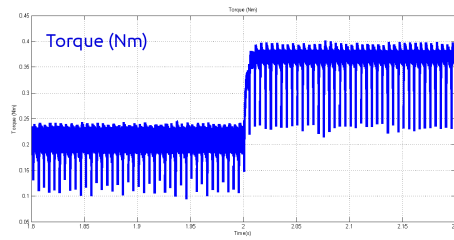
The above simulations are done with sensored control of BLDC machine. Similar results are obtained with sensorless mode of operation. The study of simulation provides deep insight of the operation of BLDC machine.



(a) Phase Current of the motor when $T_l = 0.26\text{Nm}$ is applied at $t = 2\text{s}$
Scale: x-axis- 50 ms/div , y-axis- 2 V/div



(b) Reference Vs Actual Speed
Scale: x-axis- 100 ms/div , y-axis- 1 rad/div



(c) Electromagnetic Torque developed in the motor when $T_l = 0.26\text{Nm}$ is applied at $t = 2\text{s}$
Scale: x-axis- 50 ms/div , y-axis- 50 mN/div

Figure 2.15: Sensored Operation of BLDC in Closed loop with $V_{dc} = 12\text{ V}$ and $T_l = 0.26\text{ Nm}$

CHAPTER 3

Hardware Implementation

3.1 Introduction

The modern -day power electronics is evolved with various cutting-edge technologies and compactness of components. As package dimensions reduces, thermal management becomes critically important. The effective way of dissipating heat is by forced convection (i-e)moving the air inside and around the heat source. This is achieved with the help of fans, particularly BLDC motors because of their high power-to-volume ratio. Operating the fan in full-speed leads to noisy and this condition might not needed always. This creates a demand for adjusting the speed of the fan according to environmental conditions. The real challenge of design and develop the inverter and controller circuit had been started. Our objective is to build a low cost inverter and controller circuit for BLDC machine which can be used in fan applications^[5]. Literature Survey had been carried out and found that implementing digital control of BLDC machine is cheap and effective with respect to operation. The BLDC motor with input voltage of 12 V DC is the most commonly used. We selected BLDC motor of rating 24 V, 80 W, 1500 RPM since our inverter can drive motor upto 120 W.

The digital controller for BLDC motor control is developed by various manufacturers such as Atmel, Allegro, Freescale semiconductors, Microchip Technologies, NXP Semiconductors, Renesas, Texas Instruments and Zilog etc. We have chosen PIC16LF1937 from Microchip Technologies since it has some unique features and high value to cost. PIC16LF1937 has following features.

1. 16KB of Flash Program Memory
2. 1024 Bytes of Random Access Memory (RAM)
3. 10-bit resolution and 14-channel Analog to Digital Converters (ADC)
4. Integrated Liquid Crystal Display (LCD) driver

5. Integrated Capacitive Sensing Module

6. Supports Serial-Parallel Interface(SPI), Inter-Inter Communication(I2C), Enhanced Universal Synchronous Asynchronous Receiver Transmitter (EUSART)

In this Chapter, we will briefly discuss about the design and development of controller and inverter circuit for BLDC machine and verification of experimental results.

3.2 Design of Controller Circuit

The Controller circuit for BLDC machine consists of microcontroller as its heart and Peripheral circuit required for powering the microcontroller in addition to General Purpose Input/Output pins as shown in figure 3.1. Hall sensor signals from the motor or Virtual hall sensor signals generated by back-emf sensing, are fed into the microcontroller ADC port pins as inputs. The Current signal and the DC bus voltage sense signal are also fed into microcontroller as inputs. The gating pulses are generated and taken out as outputs. The measured and estimated quantities of the machine such as reference speed, actual speed and hall frequency are displayed using 16 * 2 alphanumeric type LCD. Also, the speed response can be seen using frequency to voltage converter.

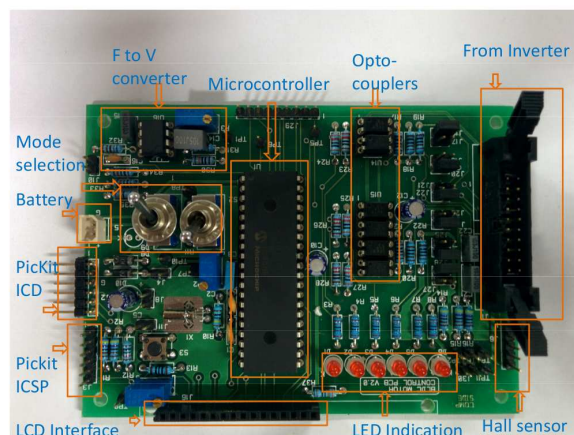


Figure 3.1: Hardware Board of Controller circuit

3.2.1 Selection of Microcontroller and its Powering modes

Microcontroller determines the speed of operation of the control algorithm, number of parameters and manipulations can be handled, starting sequence for motor and type of response when fault is detected.

Brief comparison of Microcontroller comparison from three manufacturers such as Atmel, Freescale, Microchip and Zilog as shown in table 3.1.

Table 3.1: Comparison of features of Microcontroller among different manufacturers

Features	Atmel ATtiny861	Freescale MC68HC908MR32	Microchip PIC16LF1937	zilog Z16FMC32AG20EG
Clock Frequency	20 MHz	32 MHz	32 MHz	20 MHz
Flash Memory	8 KB	Available in 16KB and 32KB	16KB	Available in 16KB and 32KB
Program Memory Instruction length	16-bit	16-bit	14-bit	16-bit
Data Memory Instruction length	512 Bytes 8-bit	768 Bytes 8-bit	1024 Bytes 8-bit	2KB 8-bit or 16-bit
Peripheral Timer Counters	One 8/16-bit One 8/10-bit Timer	Six 16-bit Timer	One 16-bit Three 8-bit Timer	Three 16-bit Timer
ADC Channels	10-bit 11 Channels	10-bit 10 Channels	10-bit 14 Channels	10-bit 12 Channels
PWM Channels	3 Channels with separate Comparators	6 Channels 12-bit modules	5 Channels Capture Comparators	6 Channels 12-bit modules
General Purpose I/O	16 pins	44 pins	36 pins	46 pins
Communication Interfaces	Universal serial with start condition detector	Serial Parallel Interface	I2C, SPI USART Interface	I2C, SPI USART Interface

From the above comparison, it is found that Microchip microcontroller has good features which can be used for motor control applications. Hence, we decided to use PIC16LF1937 for BLDC motor control. An external crystal oscillator (32.768 kHz) is provided so that user can make use of it if internal oscillators are not working.

3.2.1.1 Powering Modes of Microcontroller

There are three modes of powering up the microcontroller ^[8] as shown in figure 3.2.

1. PicKit 3 In-Circuit Debugger (ICD)
2. PicKit In-Circuit Serial Programmer (ICSP)
3. 3.3V DC Power source

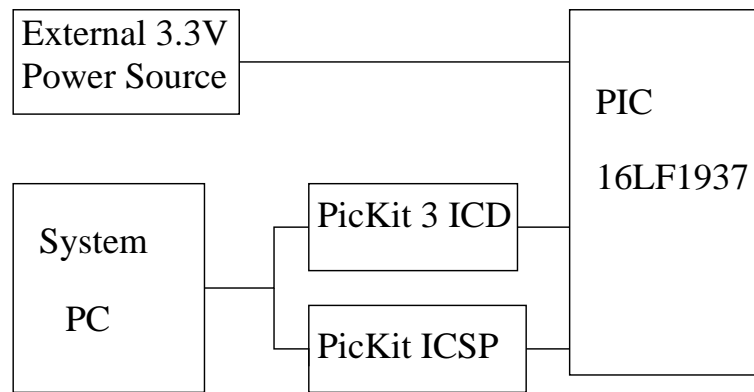


Figure 3.2: Powering Options of Microcontroller

PicKit 3 ICD cum Programmer provides powering, programming the microcontroller and debugging the coded program in the board itself. PicKit 3 ICD should be connected to system or Personal Computer and there is a provision in the software where we can have the option of powering the board from PicKit 3 ICD. MPLAB X Integrated Development Environment (IDE) is the software where we can edit the program in C or assembly, compile the program and build the program. Then we have to select the target device for programming and debug the program in MPLAB which enables the PicKit 3 ICD to operate in debugging mode.

3.2.1.2 Description about MPLAB X IDE software

MPLAB X IDE is a free software provided by Microchip along with MPLAB X Compilers. MPLAB X supports 8-bit, 16-bit microcontrollers and dsPIC digital signal microcontrollers. MPLAB X simulator where we can simulate the entire hardware circuit and watch the variable values in the watch window. Thus, MPLAB X IDE is a very effective tool in terms of programming and debugging the program. The MPLAB X IDE supports different compilers such as Hi-tech C, MPASM, PIC C compiler and XC8, XC16, C32 compilers. The set of procedure to be followed for creating new project, editing the source file and building the program. Finally, we have to debug the program so that it programs the target device and enters debugging mode. The program can also be dumped into flash memory and after that there is no requirement of programmer. The basic gate pulse is as shown in figure 3.3.

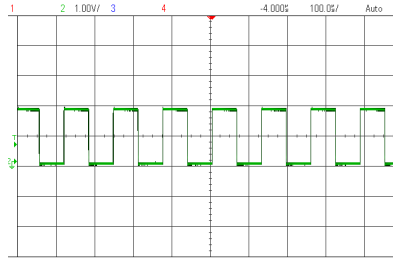


Figure 3.3: Basic Gate Pulse from microcontroller
Scale x-axis - 10 μ s/div y-axis - 1 V/div

3.3 Design of LCD interface

PIC16LF1937 microcontroller has integrated LCD driver which supports seven segment display. The Timer 1 can be used to clock the LCD module and microcontroller itself provides the power. The maximum range of the microcontroller is $4\frac{1}{2}$ digit. Due to the non-availability of segmented LCD, we have moved to alphanumeric LCD. 16*2 display is the most commonly used. The power for LED backlit and LCD circuit is provided by external 5 V adaptor.

3.4 Implementation of Frequency to Voltage converter

If reference speed is changed at time instant, say t sec, the time taken by the actual speed to track the reference speed is known as the response time of the system. The hall signals which give information about the angular velocity of the rotor is given to frequency to voltage converter and corresponding output is proportional to the input frequency. Here We used KA331 which is a Voltage to Frequency converter, also can be configured as Frequency to Voltage converter. The full scale range of frequency is 10 kHz. The supply given to IC is 5 V. The output consists of low-pass filter whose cut-off frequency should be such that the rise time of the speed response should not be affected.

3.5 Software Implementation

The clock frequency is 32 MHz and instruction frequency is $f_{osc} / 4$ (i-e) 8 MHz. The microcontroller has an excellent capability of handling interrupts with automatic context saving.

There are two routines by which program is executed. The main routine where all the variable declaration and LCD initialization codes are written.

The interrupt service routine consists of the gate pulse generation logic and closed loop control implementation code. The ISR will provide constant execution frequency and it is set to 40 kHz.

The entire program is written in C program. The Registers, Timers and other microcontroller peripherals are initialized with the syntax as per device datasheet.

The basic block diagram depicts the sequence of initialization of software is as shown in figure 3.4.

The inclusion of necessary header files to the program should be done first. For displaying the characters in LCD, Analog to Digital conversion, Button input for mode switching,

Also the configuration words should be initialized properly at the beginning. Master clear reset, Watch-dog timer, Brown-out reset are set appropriately.

The algorithm for writing the main loop^[6] is given as in figure 3.5.

The main routine consists of setting up of all Timers, Registers and Interrupts. Then, the LCD routine is initialized and switching between display modes when button input is sensed. The display of characters and values of the parameters are written in the LCD routine.

The algorithm for writing the interrupt service routine^[7] is given in figure 3.6.

The interrupt service routine is executed when capture input pin of the microcontroller

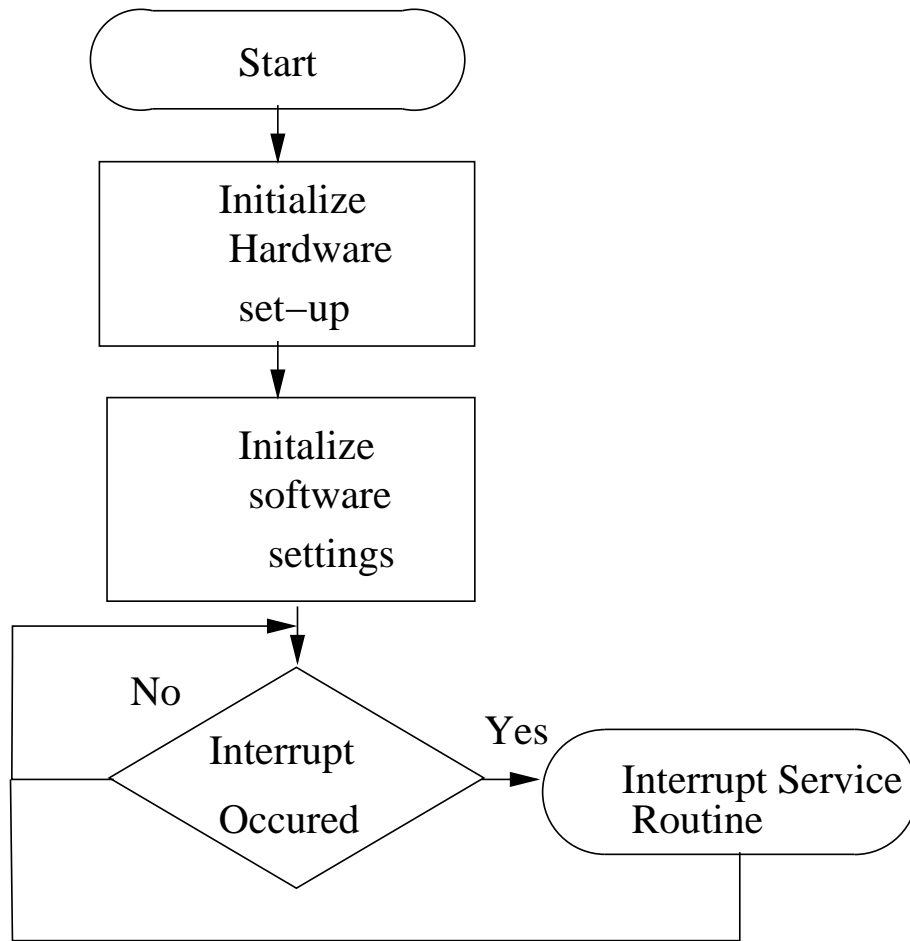


Figure 3.4: Main Procedure for running experiment

senses the every rising edge of the signal and Timer overflows. The speed is calculated based on the consecutive rising edges and counter value between two edge sensing. Also Timer 0 is used for running the control sequence and commutation sequence functions at constant sampling time.

3.6 Design of Inverter Circuit

The BLDC machine is driven by three-phase inverter bridge circuit. The topology of the inverter is 2-level Voltage Source inverter. Conventionally, all six power switches used in the inverter bridge circuit are N-Channel MOSFETs. MOSFETs are chosen for low power high frequency applications whereas for high power and low frequency applications, Insulated gate Bipolar Transistors (IGBT) are used.

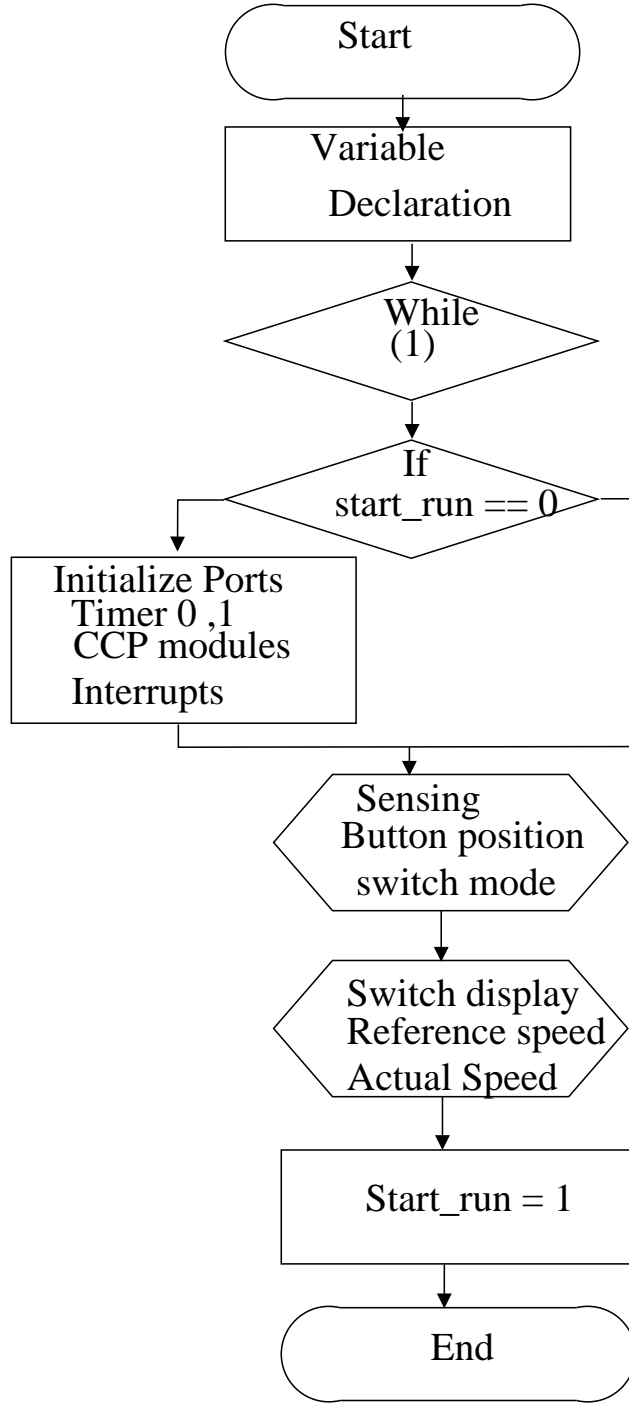


Figure 3.5: Algorithm for Main loop

The circuit diagram of two level Voltage Source Inverter is as shown in figure 3.7.

The pole voltage at the midpoint of each leg of the inverter takes only two values either V_{dc} or zero.

$$V_{aN} = U_a * V_{dc} \quad (3.1)$$

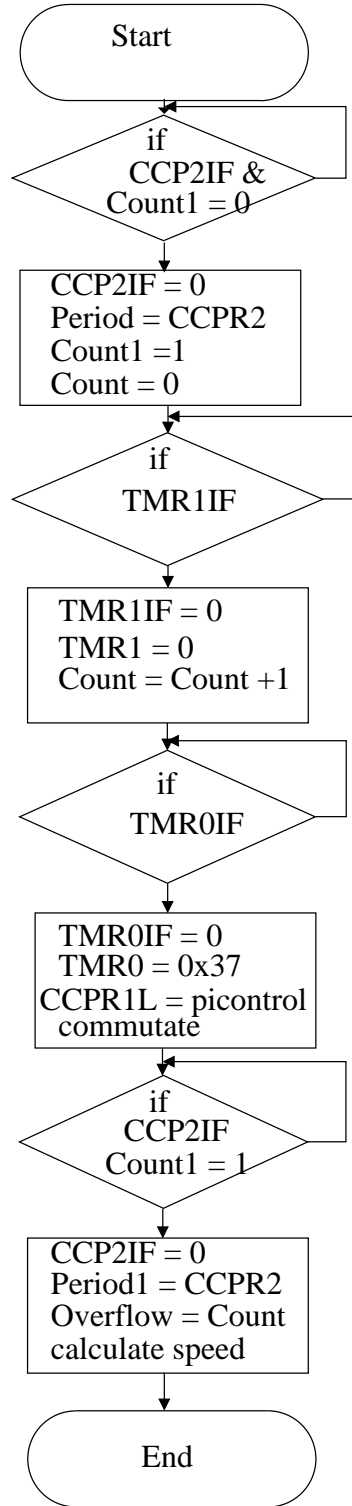


Figure 3.6: Algorithm for Interrupt Service Routine loop

where, $U_a = 1$ when switch S1 is ON and $U_a = 0$ when switch S4 is ON

Similarly, for V_{bN} and V_{cN}

The phase voltage of the machine is given by

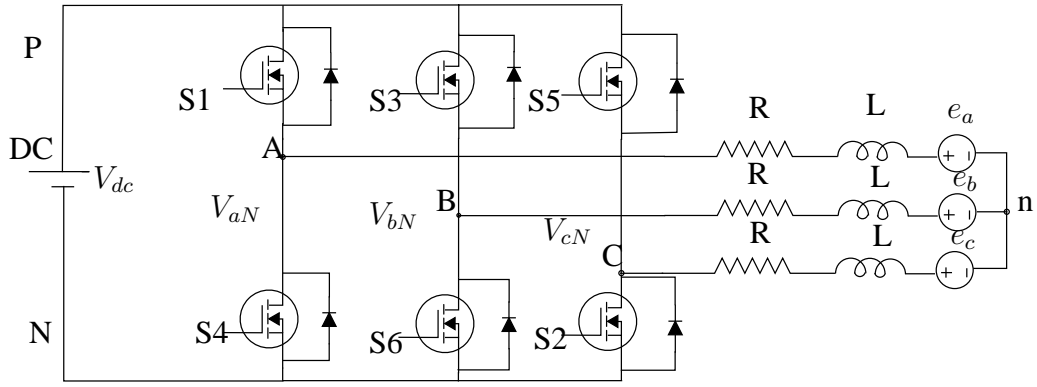


Figure 3.7: Typical 2-level Voltage Source Inverter

$$V_{an} = V_{aN} + V_{Nn} \quad (3.2)$$

Similarly for V_{bn} and V_{cn}

$$V_{Nn} = -\frac{(V_{aN} + V_{bN} + V_{cN})}{3} \quad (3.3)$$

The phase voltage of the machine can be represented in terms of DC bus voltage V_{dc} as shown below

$$V_{an} = S_a * V_{dc} \quad (3.4)$$

where, Switching function $S_a = \frac{1}{3} * (2U_a - U_b - U_c)$

similarly for V_{bn} and V_{cn}

For low voltage applications where V_{DS} less than 200 V, Power Trench MOSFETs are used instead of conventional planar MOSFETs. Power Trench MOSFETs have vertical structure of inner layers and they are compact devices compared to planar MOSFETs. With the implementation of CMOS technology, the gate threshold voltage has been reduced to 2 V for 10-15 V V_{DS} applications.

From figure 3.8, the gate threshold voltage characteristics of N-Channel MOSFET (DMN3007LSS) is measured and found it to be 1.9 V.

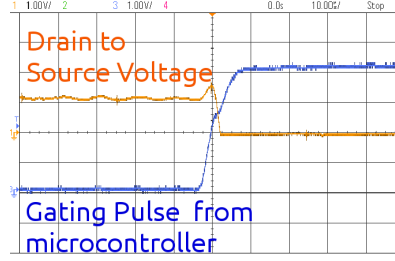


Figure 3.8: Gate Turn-ON characteristics of N-channel MOSFET
Scale x-axis -10 μ s/div y1-axis -1 V/div y2-axis -1 V/div

From figure 3.9, the gate threshold voltage characteristics of P-Channel MOSFET (IRF9317PbF) is measured and found it to be 2.1 V.

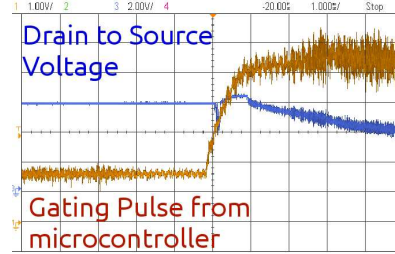


Figure 3.9: Gate Turn-ON characteristics of P-channel MOSFET
Scale x-axis - 1 ms/div y-axis - 2 V/div y2-axis - 1 V/div

Conventionally, Six N-Channel MOSFETs are employed which has high mobility rate of charge carriers and low R_{DS} compared to P-Channel MOSFETs. The major drawback of N-Channel MOSFETs is that they require isolated gate drivers or pulse transformers for high and low-side switches, which will make the circuit complex. This requires additional power supply and saturation effects of transformers. To overcome the above issues, P-Channel MOSFETs as high side switches where low-side gate driver can be used with simple level shifting.

The main disadvantage of P-Channel MOSFET is high R_{DS} (on) and about three times lesser mobility rate of charge carriers. For same R_{DS} , the size of P-Channel MOSFET is bigger than N-Channel MOSFET. This means the cost-effective solution with P-Channel MOSFETs require optimization of devices towards reduced R_{DS} . For low frequency applications, bootstrap loader or floating gate driver circuit is used.

The ratings and specifications of the MOSFETs are attached in Appendix.

3.6.1 Design Consideration for transistor driver configuration in BLDC Inverter Circuit

From the circuit diagram shown in figure 3.10,

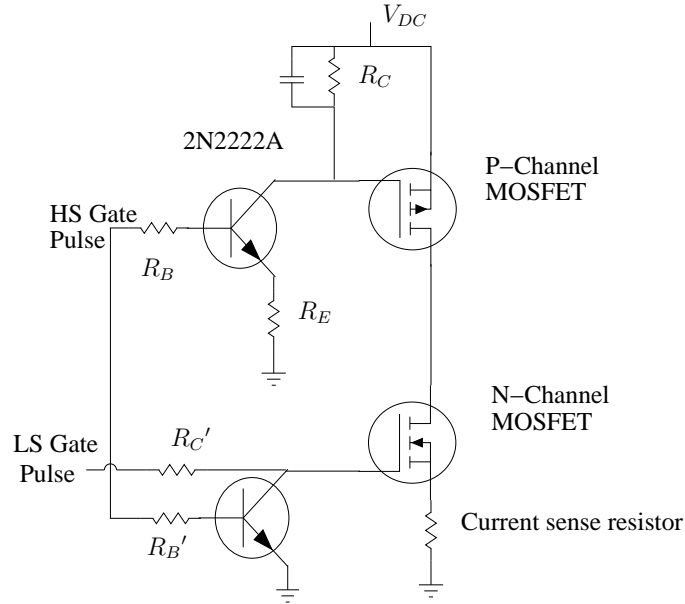


Figure 3.10: Transistor Driver circuit for MOSFETs

Applying KVL for Base-Emitter Loop

$$V_{BB} - I_B R_B - V_{BE} - I_E R_E = 0 \quad (3.5)$$

DC current gain of NPN transistor is given by

$$\begin{aligned} \beta &= \frac{I_C}{I_B} \\ I_C &= \beta I_B \end{aligned} \quad (3.6)$$

We know,

$$I_E = I_C + I_B \quad (3.7)$$

where $I_B \ll I_C$

So

$$I_E \approx I_C \quad (3.8)$$

$$I_E = \beta I_B \quad (3.9)$$

By using the above equations

$$3.3 - I_B R_B - 0.7 - \beta I_B R_E = 0 \quad (3.10)$$

$$2.6 = (R_B + \beta R_E) I_B$$

$$I_B = \frac{2.6}{(R_B + \beta R_E)}$$

where $R_B \ll \beta R_E$

$$I_B \approx \frac{2.6}{\beta R_E} \quad (3.11)$$

$$I_C \approx \frac{2.6}{R_E} \quad (3.12)$$

$$(3.13)$$

The above transistor circuit configuration is known as Emitter Bias Configuration. It has the following advantages.

- 1) It provides degeneration, negative feedback effect.
- 2) It assures the stability (i.e) Stabilizes the Q-Point of the transistor.

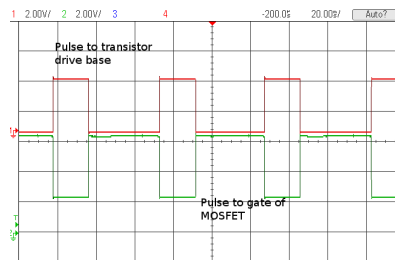


Figure 3.11: Driver output with respect to gate pulse
Scale x-axis - 20 ms/div y-axis - 2 V/div

Applying KVL for the collector Emitter Loop

$$V_{CC} - I_C R_C - V_{CE} - I_E R_E = 0 \quad (3.14)$$

$$V_{CC} - I_C R_C - V_{CE} - I_C R_E = 0$$

$$V_{CC} - V_{CE} = I_C (R_C + R_E)$$

$$I_C = \frac{24 - V_{CE}}{(R_C + R_E)}$$

$$I_B = \frac{24 - V_{CE}}{\beta(R_C + R_E)}$$

Consider the following assumptions

$$I_C R_C = 5V \quad (3.15)$$

$$I_E R_E = 2.6V$$

$$I_C R_E \leq 2.6V$$

$$V_{CC} - V_{CE} - I_C (R_C + R_E) = 0$$

$$V_{CE} = V_{CC} - I_C (R_C + R_E)$$

$$= 24 - (5 + 2.6)$$

$$= 24 - 7.6$$

$$V_{CE} = 16.4V$$

$$(3.16)$$

This shows that the transistor is operating in active region.

$$\frac{R_C}{R_E} = \frac{5}{2.6}$$

$$R_C = 1.2R_E$$

$$(3.17)$$

The Typical value of $R_B = 1k\Omega$. By reference to the V_{CE} Vs I_C Characteristics of 2N2222A Data sheet and DC Load line characteristics, we can say that $I_C \approx 15mA$.

So,

$$\begin{aligned}
 I_B &= \frac{I_C}{\beta} \\
 &= \frac{15mA}{200} \\
 I_B &= 75\mu A \\
 R_C &= \frac{5}{15mA} \\
 &= 0.333 \times 10^3 \\
 &= 333\Omega
 \end{aligned} \tag{3.18}$$

(3.19)

So we can choose, $R_C = 330\Omega$

$$\begin{aligned}
 I_E &= I_C + I_B \\
 &= 15mA + 0.075mA \\
 I_E &= 15.075mA \\
 I_E R_E &= 2.6 \\
 R_E &= 172.47
 \end{aligned} \tag{3.20}$$

(3.21)

So we can choose $R_E = 180\Omega$ $R'_B = R_B = 1k\Omega$ To limit the current flowing into the Gate-Source capacitance C_{GS} of low-side N-Channel MOSFET, resistance of 100Ω is connected in series to the gate. So $R'_C = 100\Omega$

3.6.2 Design of Current sense resistor

The sensing of motor current is required in order to derive the control algorithm for torque control while loading the machine. Minimum of two phase current measurement should be done by placing the current meters in series to the motor terminals. Otherwise, current sensing can be done between DC power source and inverter. There are different modes of measuring the current flows to the machine.

1. Current sense resistor (Shunt resistor)
2. Current transformers
3. Hall effect sensor

Current sense resistor provides the measurement of the current at low cost with good accuracy^[8]. The Current sense resistor should be non-inductive and the value is chosen in such a way that under full load condition, the measured value should be within the range of ADC requirements. The Current sense resistor technique is limited to the measurement of current range of 20 A as power dissipation increases, beyond that. The effect of value of current sense resistor is analyzed and as shown in table 3.2.

Table 3.2: Selection of Current sense resistor value

S.No	Property	Low R_{sense}	High R_{sense}
1	Accuracy	Low	High
2	Voltage drop	Low	High
3	EMI and Noise	Low	High
4	Output range	Limited	Full scale

Metal film resistors are normally preferred to wire wound resistors, which have large inductance values. Also, sense resistors can be formed from trace resistance on a PCB. However, their accuracy over a wide temperature range is poor. The current sense resistor can be placed in high side (i-e) Positive DC bus side or low side (i-e) Negative DC bus side. Each has its own advantages and disadvantages as shown in table 3.3. Here, Current sense resistor value = 0.1Ω . The signal is isolated and amplified in

Table 3.3: Placement of Current sense Resistor

S.No	Property	Low side R_{sense}	High side R_{sense}
1	Grounding and EMI	Impact on output	Not affected
2	Output type	Single-ended	Double-wired
3	Isolation	Not required	Must required
4	Implementation	Easy	Difficult

order to meet ADC requirement of microcontroller. The schematic diagram of signal processing of sensed current signal is as shown in figure 3.12.

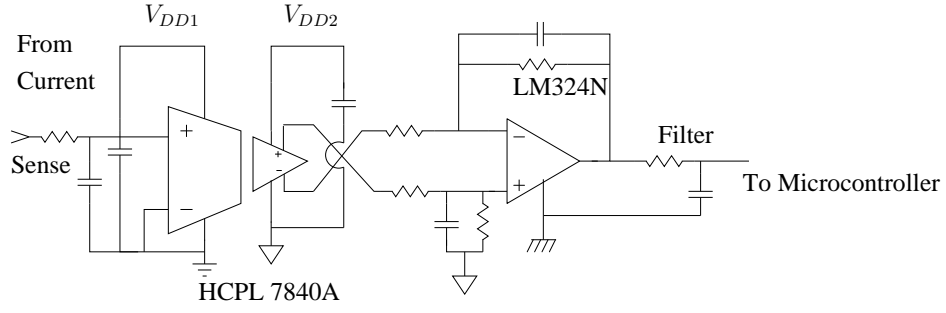


Figure 3.12: Schematic Diagram of Current sensing

3.6.3 Deign of DC bus Capacitance

The DC power source output is connected to the inverter where switching provides non-linear loading. Hence, Source is subjected to high harmonic content and it will affect the reactive power supplied by the source. In addition to this, Source will have internal impedance and it will affect the switches during course of time. The value of the capacitance is chosen by

$$Capacitance C = \frac{I_{peak}}{\Delta V * f_s} \quad (3.22)$$

We have chosen $4700\mu F$, 50 V electrolytic capacitor.

3.6.4 Design of Back-EMF sensing circuit

The back-emf signals are attenuated suitably to meet ADC requirement of microcontroller by appropriately choosing potential divider resistor values and filters are required to remove Pulse Width Modulation noises.

The circuit diagram for sensing the back-emf is as shown in figure 3.13.

$$V_a = \frac{R2}{R1+R2} * V_{aN}$$

similarly for V_b and V_c

$$R2 = 22 \text{ k}\Omega$$

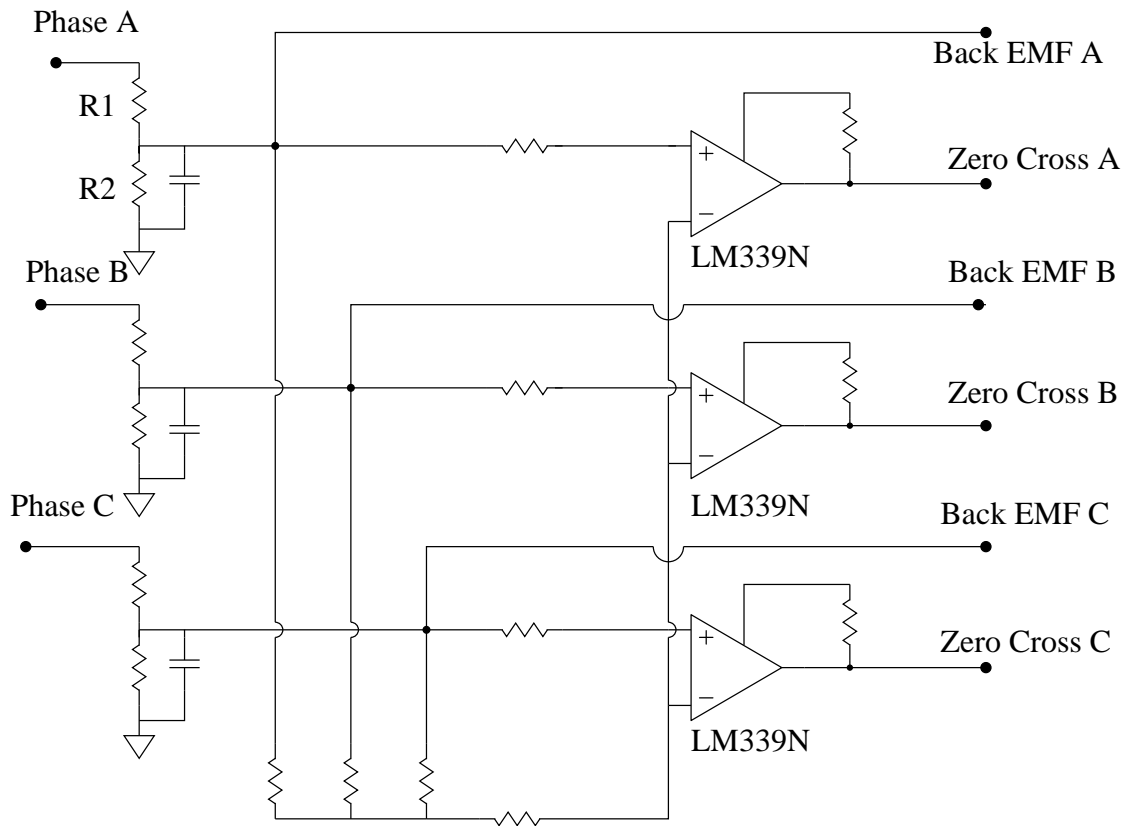


Figure 3.13: Schematic Diagram of Back EMF sensing

$R1 = 100\text{ k}\Omega$

For the Comparator, the back-emf signals are connected to non-inverting input and virtual neutral signal is connected to the inverting input. When back-emf signal is higher than virtual neutral, the comparator output will be high and vice-versa when back-emf signal is lesser.

Here, LM339N, quad channel comparator, is used which can be operated from 3 V to 36 V. The digital pulse generated from comparator output is similar to Hall sensor signals.

3.6.5 Design of Inverter Printed Circuit Board

The Inverter PCB is a double-layered having dimensions of 120 mm * 85 mm. The layout of PCB is designed in such a way that the gate drive signals are close proximity to the gate of MOSFETs and ensured the symmetry. Since the use of

practical components and tracks of appreciable length, the effect of Electromagnetic Interference is inevitable. This arises because of unwanted coupling which may be resistive, inductive or capacitive. A first order approach to reduce the effect is to follow design guidelines of PCB strictly.

As a matter of protection, fuse of 5 A is added in series to the supply line. A Low Drop-out voltage regulator is used to provide supply for the comparator ICs and Optocoupler Pull-ups.

The hardware development of inverter board is as shown in figure 3.14.

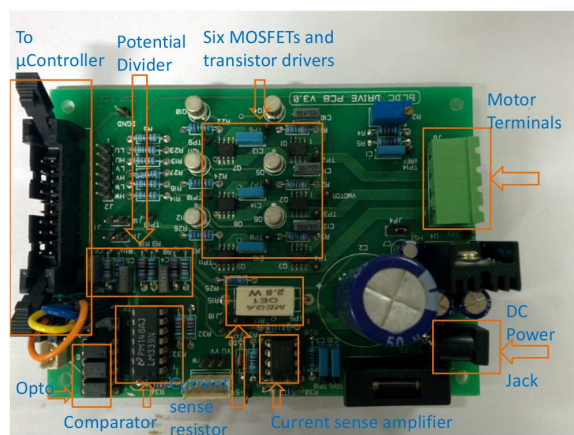


Figure 3.14: Hardware Board of Inverter circuit

3.6.6 Selection of BLDC motor

The BLDC motor with trapezoidal back-emf is available in the market from few watts to several kW ranges. The cost of the BLDC machine is high compared to equivalent rating of induction and DC machines. This is the reason due to usage of permanent magnet materials such as ferrites and rare earth magnets such as Neodymium - Ferrite Boron (NdFeB). The name plate details of the BLDC motor which we used is as follows.

1. Motor Power rating : 80 W
2. Rated Speed : 1500 RPM
3. Rated Voltage : 24 V

4. Number of Poles : 4
5. Rotor Inertia : $0.0005 \text{ kg} - m^2$

The complete set-up of the hardware is as shown in figure 3.15.



Figure 3.15: Complete Experimental set-up

The detailed specification and rating of the machine is attached in Appendix A.

3.7 Model Validation and Experimental Results

The experiment is carried with 24 V, 80 W, 1500 RPM BLDC motor, coupled with mechanical belt-drum loading arrangement as shown in figure 3.16. The Inverter board is powered from Agilent DC power source 60 V, 25 A. The microcontroller board is powered through PicKit 3 ICD which in turn connected to system or PC. The supply for the comparator IC and LCD is derived from 5 V adaptor. The waveforms are measured using Agilent 4-Channel Oscilloscope having bandwidth of 70 MHz. The measurement probes used for the experiment are Agilent 10:1 passive probe.

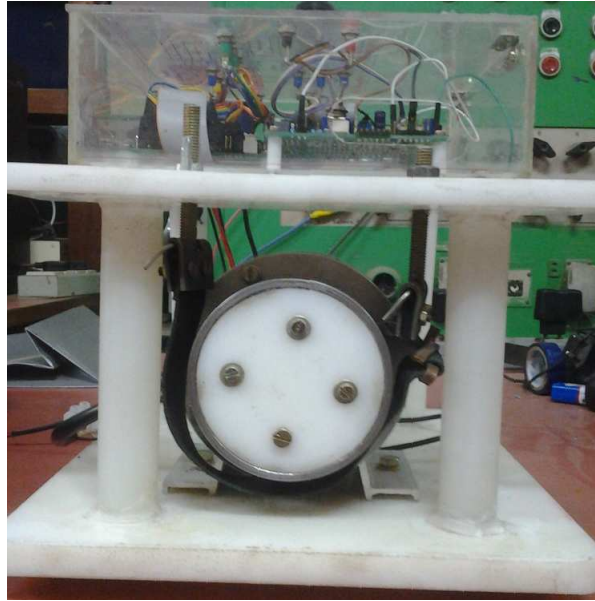


Figure 3.16: Motor loading arrangement

3.7.1 Observations and Learning outcomes from Experiments

3.7.1.1 Condition: Sensorless open loop

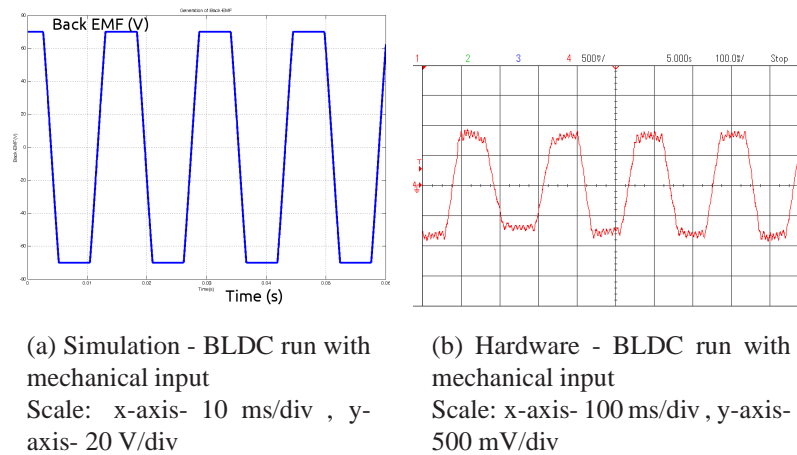


Figure 3.17: Simulation and Hardware results comparison of Motor RPM

From the figure 3.17, BLDC motor is rotated using hand as mechanical input and found the shape of the back-emf. It is observed that trapezoidal back-emf is generated and had 120° flat portion. In the hardware waveform, there are ripples in the flat portion, which is due to slot ripple. The required current excitation to the motor should be given such that constant power is developed. The power developed for the machine when rotated at

constant RPM is shown in figure 3.18b.

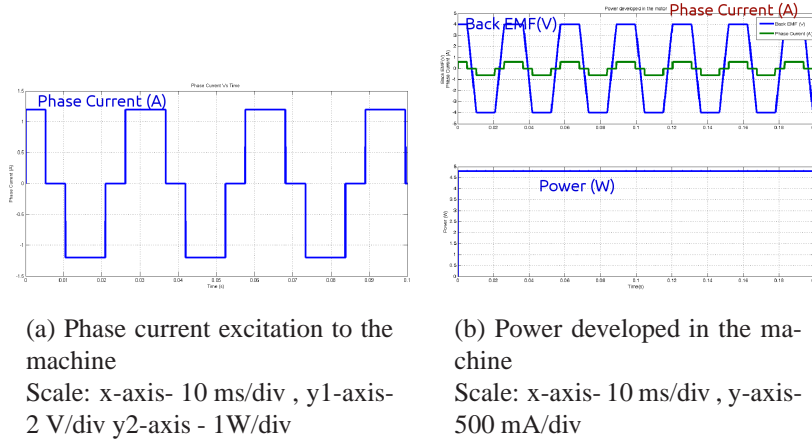


Figure 3.18: Motor Excitation current and Back EMF Voltage

This requires detection of rotor position and it is achieved using Hall sensors. The hall sensors are mounted in the stationary particularly and provided with external power source for its operation.

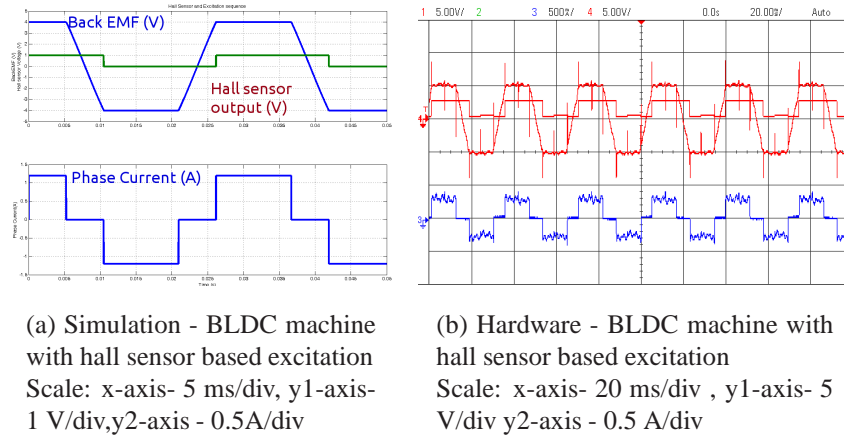


Figure 3.19: Simulation and Hardware results comparison of square wave input gate pulse

From the figure 3.19, depending upon the hall sensor outputs, the gate pulses to the MOSFETs are derived and each switch conducts for 120° and each switch combination conducts for 60° .

From the figure 3.20, it is observed that by changing PWM duty by keeping V_{DC} constant, variable output voltage can be obtained and fed to the machine. In hardware,

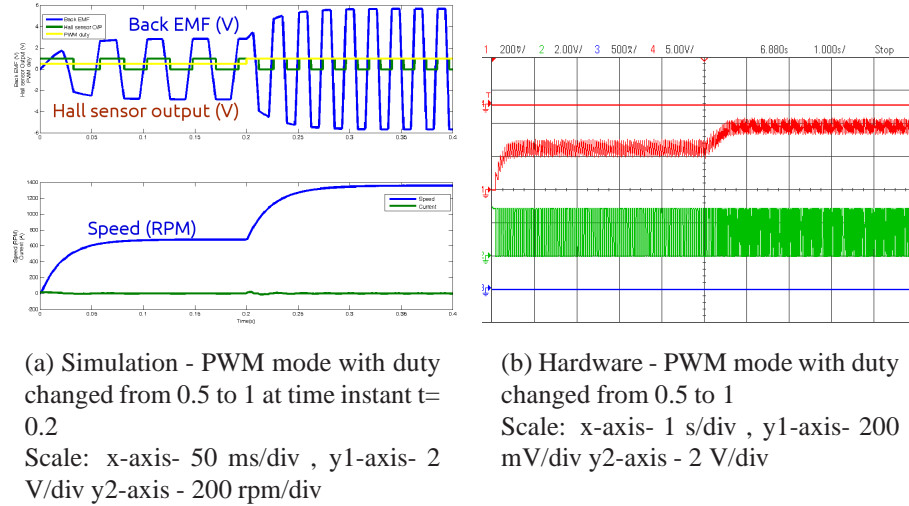


Figure 3.20: Simulation and Hardware results comparison of PWM duty to gate pulses

PWM is generated from microcontroller by setting suitable values in Timer 2 register and PWM module.

3.7.1.2 Condition : Sensorless Mode of operation in closed loop with No load

From figure 3.21a, the high side P-Channel MOSFETs are driven by square wave gate pulses without chopping. The gate pulses are phase shifted by 180° .

From figure 3.21b, the low-side N-Channel MOSFETs are driven by chopped gate pulses. The duty of the pulses are controlled by the output of Control loop.

From figure 3.21c, the phase current to the motor is measured by clamp type ammeter.

From the figure 3.22, the settling time of the speed is noted in hardware and found that around 1 s.

3.7.1.3 Condition : Sensorless mode of operation in closed loop with load

From the figure 3.23a, it is observed that the machine speed regulates to the reference speed under loaded condition. When motor load is 2.5 A, the reference speed is 800 RPM, the actual speed regulates and tracks the reference speed. From the figure 3.23b,

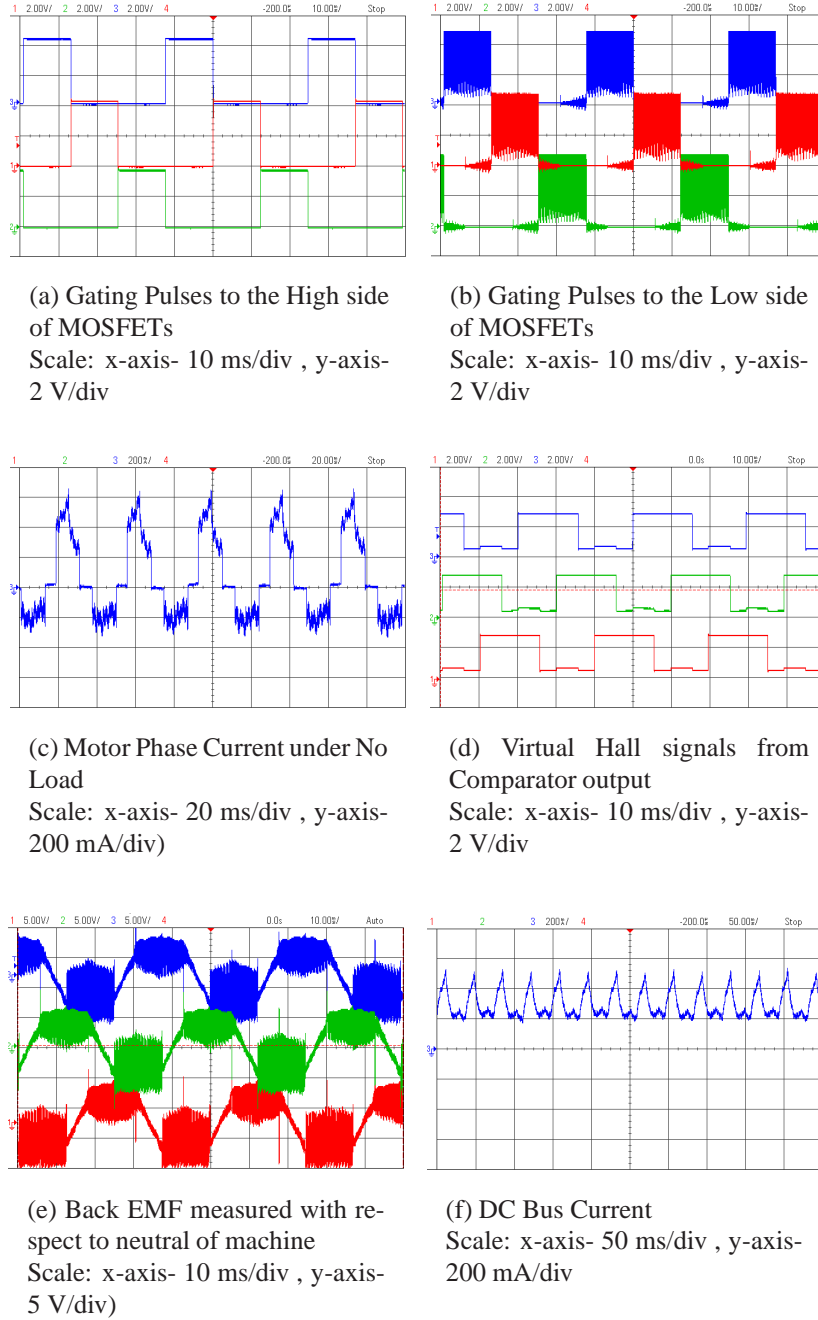
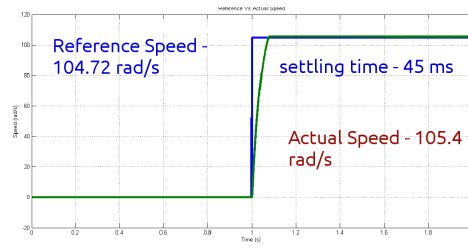


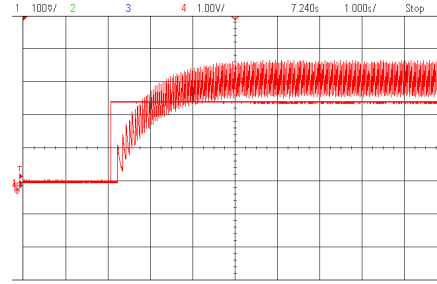
Figure 3.21: Sensorless Operation of BLDC in Closed loop with $V_{dc} = 12 \text{ V}$

it is observed that load of 2.5 A is applied instantaneously at time t sec, there is dip in the speed and then it tracks the reference speed.

Depending upon the sampling time and PI constants, the response of the control loop varies. We have implemented only speed loop which is the outer loop. The Reference speed is given by the Potentiometer whose value is converted through ADC. The LCD is used to indicate the reference speed, actual speed and Hall frequency. Thus, We have

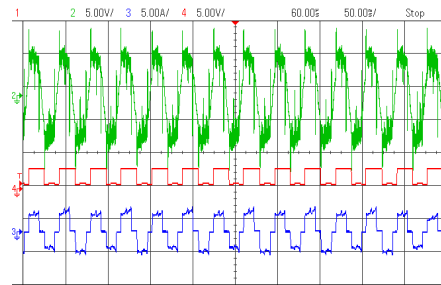


(a) Reference Vs Actual Speed
Scale: x-axis- 200 ms/div , y-axis- 20 rad/div

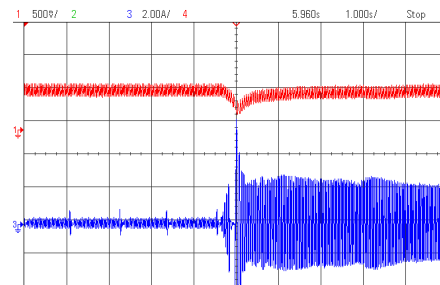


(b) Hardware - Actual Speed with pseudo reference
Scale: x-axis- 1 s/div , y-axis- 100 mV/div

Figure 3.22: Simulation and Hardware results comparison



(a) Motor Phase Current with load
Scale: x-axis- 50 ms/div , y1-axis- 5 V/div y2-axis - 5V/div y3-axis - 5A/div



(b) Hardware - Actual Speed with load disturbance
Scale: x-axis- 1 s/div , y1-axis- 500 mV/div y2-axis - 2A/div

Figure 3.23: Simulation and Hardware results comparison in loaded condition

completed the experimental validation of the hardware. Further, Inner Current loop will be closed and speed response will be plotted. Along with simulation, the verification of hardware circuit and validation of results with simulation make things understand very clearly.

CHAPTER 4

Summary and Future Scope

4.1 Summary

By carrying out this project, there are lot of learnings and good hands-on experience of hardware.

1. Initially with the study of permanent magnet materials and machines made up of permanent magnet materials, the importance of PM machines in modern-day applications has increased.
2. Permanent Magnet Brushless DC machines are similar to DC machines without commutator and brush arrangement. The modeling of BLDC machine using steady state condition and observe the performance of machine in various modes of operation in Simulink in MATLAB.
3. The design of controller for achieving the speed regulation and torque ripple reduction under sudden loading conditions. The selection of bandwidth for both inner loop and outer loop depending upon the constraints of the machine modeling has been studied.
4. The development of circuit reveals the non-idealities associated with ideal conditions assumed for theoretical and simulation. The effect of temperature, electromagnetic interference, inductive and capacitive coupling which is not considered in theoretical and simulation will play a crucial role in achieving the output.

4.2 Future Scope

The future scope of this work includes the implementation of four quadrant PMDC drive with the same inverter and controller board.

The inverter circuit is slightly modified with line driver ICs and inclusion of delay card in the controller make the entire circuit versatile to be used for induction drives.

In the view of low-cost development, an application specific ICs can be used which consists of Hexfet MOSFET bridge along with driver and protection circuits.

APPENDIX A

Motor Specifications

TARUN TECHNOLOGIES									
SPECIFICATION									
Frame	IIT	IP	23	Espec No.		spec			
kW	0.08	IC	o1	CONFORMING SPEC					
Volts	24	rpm	2630	GENERALLY					
current	4.43	Hz	100.00	TESTING					
Ph	2	Ins Cl	F	Duty		S1			
STATOR		ROTOR		Permanent magnet					
STAMPING MATERIAL		rotealloy		0.3		Magarc(deg)		90	
STATOR SLOTS		24				Mag wt(kg)		0.37	
STAMPING WEIGHT (kg)		1.4				tit sleeve(mm)		0.1	
CORE LENGTH		60				Airgap(mm)		0.7	
Stator out sde dia		90				Mag OD(mm)		43.4	
STATOR INSIDE DIA (mm)		45				magnet thick		20.00	
						Magnet ID		3.40	
						st od		90	
STATOR WINDING		SW G		no of		DIAMETER		CU WT (kgs)	
PITCH		1to4		COND DIA 1		20		2	
WINDING		CONCENTRIC		COND DIA 2		0		0	
LMT		0.34		COND DIA 3		0		0	
T/ci single L		9				0		4	
CONNECT		STAR		gr/ph		gr		coils/gr	
R/PHASE		0.15369						no of layers	
L stat mh/ph		0.16						1	
slot fill		17.88		INPUT		losses		Out put	
VOLTAGE		24		93		12.82		80.00	
								0.86	

Figure A.1: Motor Specification

APPENDIX B

Circuit Block Diagram

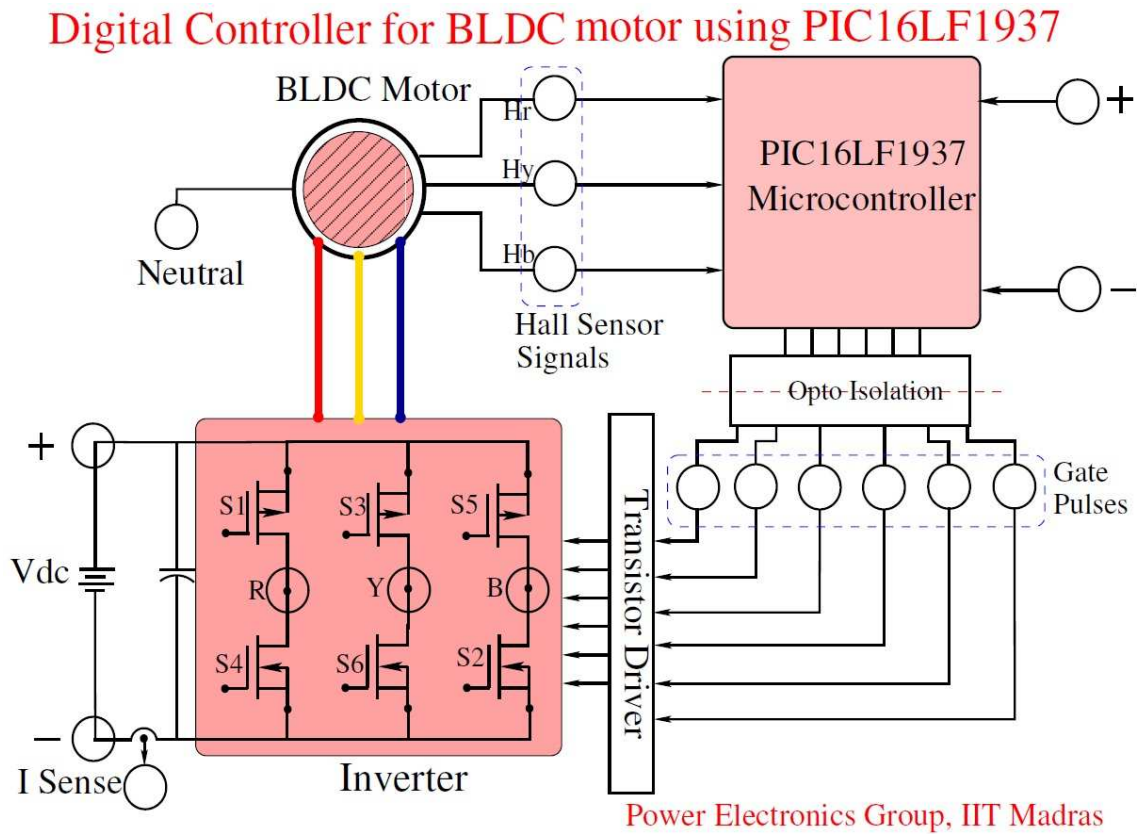


Figure B.1: Complete Circuit Block Diagram

APPENDIX C

Inverter Schematic

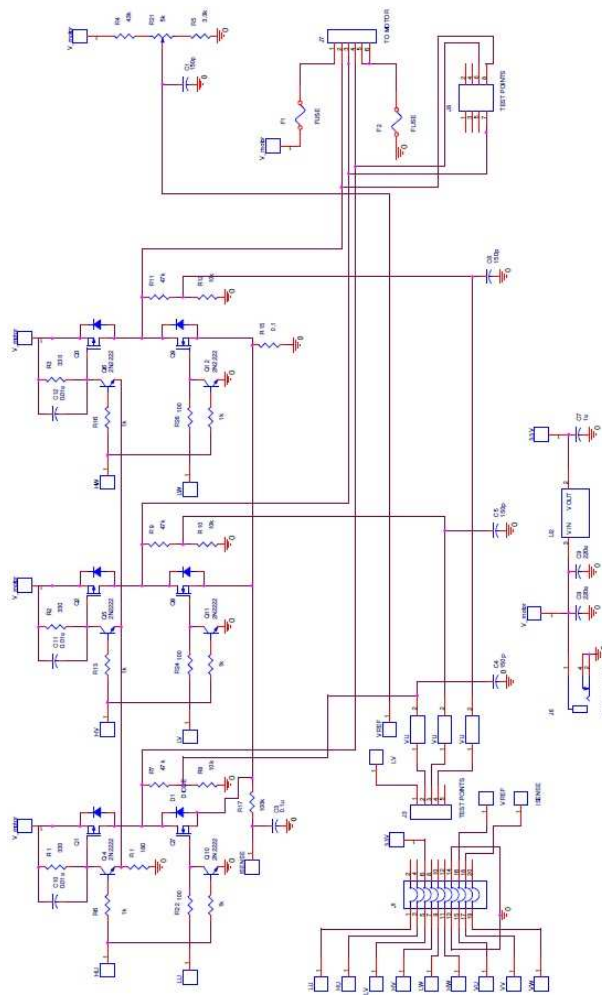


Figure C.1: Inverter Schematic for BLDC Drive

Controller Schematic



APPENDIX E

Bill of Materials for Driver Circuit

S.No	Item	Symbol	Specifications	Part Number	Quantity
1	Resistors	R5,R6,R13,R16,R23,R25,R27,R28,R30	1k, 1/4W	Discrete	9
2	Resistors	R1,R2,R3	330,1/4W	Discrete	3
3	Resistors	R22,R24,R26	100,1/4W	Discrete	3
4	Resistors	R7,R9,R11	47k,1/4W	Discrete	3
5	Resistors	R8,R10,R12	10k,1/4W	Discrete	3
6	Resistor	R4	6.8k,1/4W	Discrete	1
7	Resistors	R18,R19,R20	220,1/4W	Discrete	3
8	Resistor	R15	0.1,1W	Discrete	1
9	Resistor	R14	180,1/4W	Discrete	1
10	Resistors	R17,R31	100k,1/4W	Discrete	2
11	Resistor	R29	3.3k,1/4W	Discrete	1
12	Potentiometer	R21	1k,1/4W	Discrete	1
13	Capacitor	C7	1u,50V	Discrete	1
14	Capacitors	C10,C11,C12	0.01uF, 50V	Discrete	3
15	Capacitors	C4,C5,C6	0.22uF,50V	Discrete	3
16	Capacitors	C1,C2,C3,C13,C14,C15	0.1uF,50V	Discrete	6
17	Capacitors	C8,C9	220uF,50V	Discrete	2
18	Capacitor	C16	4700uF,50V	Discrete	1
19	NPN Transistor	Q4,Q5,Q6,Q10,Q11,Q12	40V, 600mA	2N2222A, TO-18	6
20	P-Channel MOSFET	Q1,Q2,Q3	30V, 16A	IRF9317PbF	3
21	N-Channel MOSFET	Q7,Q8,Q9	30V,16A	DMN3007LSS	3
22	Voltage Regulator	U1, 7805	+5V	TO-220	1
23	Comparator IC	LM339N	14-pin DIP	LM339N	1
24	Opamp IC	U14	8-pin DIP	LM741	1
25	Zener diode	D3	3.3V	3V3	1
26	Fuse	F1	250V, 5A		1

Figure E.1: BOM for Driver Circuit

APPENDIX F

Bill of Materials for Controller Circuit

S.No	Item	Symbol	Specifications	Part Number	Quantity
1	Resistors	R3,R4,R5,R6,R7,R8,R11	180, 1/4W	Discrete	7
2	Resistors	R1,R2,R14,R15,R16	4.7k,1/4W	Discrete	5
3	Resistors	R13	100,1/4W	Discrete	1
4	Resistors	R17,R18,R19,R20,R21,R22,R37	1k,1/4W	Discrete	6
5	Resistors	R12,R33,R34	10k,1/4W	Discrete	3
6	Resistor	R10	10M,1/4W	Discrete	1
7	Resistors	R23,R24,R25,R26,R27,R28	150,1/4W	Discrete	7
8	Resistor	R30	100k,1/4W	Discrete	1
9	Resistor	R32	6.8k,1/4W	Discrete	1
10	Resistors	R31	15k,1/4W	Discrete	1
11	Resistor	R35	68k,1/4W	Discrete	1
12	Potentiometers	R9,R29	10k,1/4W	Discrete	2
13	Potentiometer	R36	5k,1/4W	Discrete	1
13	Capacitor	C6	1u,50V	Discrete	1
14	Capacitors	C8	0.01uF, 50V	Discrete	1
15	Capacitors	C3,C4,C5,C9	0.1uF,50V	Discrete	4
16	Capacitors	C1,C2	12pF,50V	Discrete	2
17	Capacitors	C10 to C21	1n,50V	SMD	12
18	Capacitor	C7	470pF,50V	Discrete	1
19	Optocoupler	U14	DIP - 8	TCET 2100	1
20	Optocoupler	U15	DIP - 16	TCET 4100	1
21	V-F Converter	U16	DIP-8	KA331	1
22	LED	D1 to D6, D9	Discrete	Red	7
23	Diode	D7,D8	DO - 41	1N4007	2
24	SPST Switch	S1,S2			2
25	PUSH DC Switch	U8			1
26	Microcontroller	U1	40-pin DIP	PIC16LF1937	1
27	Crystal	X1	32.768kHz		1

Figure F.1: BOM for Controller Circuit

APPENDIX G

N Channel MOSFET



DMN3007LSS

Electrical Characteristics @T_A = 25°C unless otherwise specified

Characteristic	Symbol	Min	Typ	Max	Unit	Test Condition
OFF CHARACTERISTICS (Note 5)						
Drain-Source Breakdown Voltage	BV _{DSS}	30	—	—	V	V _{GS} = 0V, I _D = 250μA
Zero Gate Voltage Drain Current	I _{DSS}	—	—	1	μA	V _{DS} = 30V, V _{GS} = 0V
Gate-Source Leakage	I _{GSS}	—	—	±100	nA	V _{GS} = ±20V, V _{DS} = 0V
ON CHARACTERISTICS (Note 5)						
Gate Threshold Voltage	V _{GS(th)}	1.3	—	2.1	V	V _{DS} = V _{GS} , I _D = 250μA
Static Drain-Source On-Resistance	R _{DS(on)}	—	5 7.9	7 10	mΩ	V _{GS} = 10V, I _D = 15A V _{GS} = 4.5V, I _D = 13A
Forward Transconductance	g _{fs}	—	16.4	—	S	V _{DS} = 10V, I _D = 15A
Diode Forward Voltage (Note 5)	V _{SD}	—	0.67	1.2	V	V _{GS} = 0V, I _S = 2.3A
DYNAMIC CHARACTERISTICS						
Input Capacitance	C _{iss}	—	2714	—	pF	V _{DS} = 15V, V _{GS} = 0V f = 1.0MHz
Output Capacitance	C _{oss}	—	436	—	pF	
Reverse Transfer Capacitance	C _{rss}	—	380	—	pF	
Gate Resistance	R _G	—	0.7	—	Ω	V _{DS} = 0V, V _{GS} = 0V, f = 1.0MHz
SWITCHING CHARACTERISTICS						
Total Gate Charge	Q _g	—	31.2 64.2	—	nC	V _{DS} = 15V, V _{GS} = 4.5V, I _D = 16A V _{DS} = 15V, V _{GS} = 10V, I _D = 16A
Gate-Source Charge	Q _{gs}	—	7.1	—		V _{DS} = 15V, V _{GS} = 10V, I _D = 16A
Gate-Drain Charge	Q _{gd}	—	17.1	—		V _{DS} = 15V, V _{GS} = 10V, I _D = 16A
Turn-On Delay Time	t _{d(on)}	—	10.3	—	ns	V _{DS} = 15V, V _{GS} = 10V, I _D = 1A, R _G = 6.0Ω
Rise Time	t _r	—	14.8	—		
Turn-Off Delay Time	t _{d(off)}	—	85.1	—		
Fall Time	t _f	—	43.6	—		

Notes: 5. Short duration pulse test used to minimize self-heating effect.

Figure G.1: Specifications of N-Channel MOSFET

APPENDIX H

P Channel MOSFET

IRF9317PbF

International
IOR Rectifier

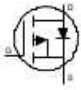
Static @ $T_J = 25^\circ\text{C}$ (unless otherwise specified)

	Parameter	Min.	Typ.	Max.	Units	Conditions
BV_{DSS}	Drain-to-Source Breakdown Voltage	-30	—	—	V	$V_{GS} = 0V, I_D = -250\mu A$
$\Delta BV_{DSS}/\Delta T_J$	Breakdown Voltage Temp. Coefficient	—	0.022	—	V/ $^\circ\text{C}$	Reference to $25^\circ\text{C}, I_D = -1\text{mA}$
$R_{DS(on)}$	Static Drain-to-Source On-Resistance	—	5.4	6.6	$\text{m}\Omega$	$V_{GS} = -10V, I_D = -16A$ ③
		—	8.3	10.2		$V_{GS} = -4.5V, I_D = -13A$ ③
$V_{GS(th)}$	Gate Threshold Voltage	-1.3	-1.8	-2.4	V	$V_{DS} = V_{GS}, I_D = -50\mu A$
$\Delta V_{GS(th)}$	Gate Threshold Voltage Coefficient	—	-5.7	—	$\text{mV}/^\circ\text{C}$	
I_{DSS}	Drain-to-Source Leakage Current	—	—	-1.0	μA	$V_{DS} = -24V, V_{GS} = 0V$
		—	—	-150		$V_{DS} = -24V, V_{GS} = 0V, T_J = 125^\circ\text{C}$
I_{GSS}	Gate-to-Source Forward Leakage	—	—	-100	nA	$V_{GS} = -20V$
	Gate-to-Source Reverse Leakage	—	—	100		$V_{GS} = 20V$
g_{fs}	Forward Transconductance	36	—	—	S	$V_{DS} = -10V, I_D = -13A$
Q_g	Total Gate Charge ③	—	31	—	nC	$V_{DS} = -15V, V_{GS} = -4.5V, I_D = -13A$
Q_{gs}	Gate-to-Source Charge ③	—	9	—	nC	$V_{GS} = -10V$
Q_{gd}	Gate-to-Drain Charge ③	—	14	—	nC	$V_{DS} = -15V$
R_G	Gate Resistance ③	—	14	—	Ω	$I_D = -13A$
$t_{d(on)}$	Turn-On Delay Time	—	19	—	ns	$V_{DD} = -15V, V_{GS} = -4.5V$ ③ $I_D = -1.0A$ $R_G = 6.8\Omega$ See Figs. 20a & 20b
t_r	Rise Time	—	64	—		
$t_{d(off)}$	Turn-Off Delay Time	—	160	—		
t_f	Fall Time	—	120	—		
C_{iss}	Input Capacitance	—	2820	—	pF	$V_{GS} = 0V$
C_{oss}	Output Capacitance	—	640	—		$V_{DS} = -15V$
C_{rss}	Reverse Transfer Capacitance	—	370	—		$f = 1.0\text{MHz}$

Avalanche Characteristics

	Parameter	Typ.	Max.	Units
E_{AS}	Single Pulse Avalanche Energy ②	—	330	mJ
I_{AR}	Avalanche Current ①	—	-13	A

Diode Characteristics

	Parameter	Min.	Typ.	Max.	Units	Conditions
I_S	Continuous Source Current (Body Diode)	—	—	-2.5	A	MOSFET symbol showing the integral reverse p-n junction diode. 
I_{SM}	Pulsed Source Current (Body Diode) ①	—	—	-130		
V_{SD}	Diode Forward Voltage	—	—	-1.2	V	$T_J = 25^\circ\text{C}, I_S = -2.5A, V_{GS} = 0V$ ③
t_{rr}	Reverse Recovery Time	—	33	50	ns	$T_J = 25^\circ\text{C}, I_F = -2.5A, V_{DD} = -24V$
Q_{rr}	Reverse Recovery Charge	—	30	45	nC	$di/dt = 100A/\mu s$ ③

Thermal Resistance

	Parameter	Typ.	Max.	Units
$R_{\theta JA}$	Junction-to-Ambient ④	—	20	$^\circ\text{C}/W$
$R_{\theta JL}$	Junction-to-Lead ④	—	50	

Figure H.1: Specifications of P-Channel MOSFET

REFERENCES

1. T.J.E.Miller., "*Brushless permanent-magnet and reluctance motor drives*", Oxford University Press, New york, 1989.
2. R. Krishnan., "*Electric Motor drives: Modelling, Analysis and Control*", Prentice Hall, Upper Saddle River, New Jersey, Third Edition, 2002.
3. Bimal K.Bose., "*Modern power electronics and AC drives*", Prentice Hall, Upper Saddle River, New Jersey, 2005.
4. Yedale Padmaraja., "*Brushless DC Motor Fundamentals*", AN885, Microchip Technology Inc, 2003.
5. Chang Liang Xia., "*Permanent magnet Brushless DC motor drives and controls*", John Wiley and Sons Press, Singapore, 2012.
6. Muhammad Ali Mazidi;Rolin D.McKinlay;Danny Causey., "*PIC Microcontroller and Embedded Systems using Assembly and C for PIC18*", Pearson International Edition, Upper Saddle River, New Jersey, 2008.
7. Han way Huang., "*PIC Microcontroller:An Introduction to Software and Hardware Interfacing*", Thomson Delmar Learning, New York, 2005.
8. Microchip., "*F1 Evaluation Platform for Enhanced PIC Microcontrollers user's*

guide”, DS41401B Microchip Technology Inc, 2010.